Published online 11 May 2010

Nucleic Acids Research, 2010, Vol. 38, No. 17 ***5909–5918***
doi:10.1093/nar/gkq335

A small nucleolar RNA functions in rRNA processing in *Caenorhabditis elegans*

Yusuke Hokii[1], Yumi Sasano[2,3], Mayu Sato[4], Hiroshi Sakamoto[5], Kazumi Sakata[6], Ryuzo Shingai[6], Akito Taneda[7,8], Shigenori Oka[3], Hyouta Himeno[1,4,8], Akira Muto[4], Toshinobu Fujiwara[2,9,*] and Chisato Ushida[1,4,8,*]

[1]Functional Genomics and Technology, United Graduate School of Agricultural Science, Iwate University, 18-8 Ueda 3-chome, Morioka 020-8550, [2]Department of Chemical Science and Engineering, Graduate School of Engineering, Kobe University, 1-1 Rokkodaicho, Nadaku, Kobe 657-8501, [3]Drug Discovery Support Technology Development Team, Research & Development Center, Nagase & Co., Ltd, 2-2-3 Murotani, Nishi-ku, Kobe, Hyogo 651-2241, [4]Department of Biochemistry and Molecular Biology, Faculty of Agriculture and Life Science, Hirosaki University, 3 Bunkyo-cho, Hirosaki, Aomori 036-8561, [5]Department of Biology, Graduate School of Science, Kobe University, 1-1 Rokkodaicho, Nadaku, Kobe, Hyogo 657-8501, [6]Laboratory of Bioscience, Faculty of Engineering, Iwate University, 4-3-5 Ueda, Morioka, Iwate 020-8551, [7]Graduate School of Science and Technology, [8]RNA Research Center, Hirosaki University, 3 Bunkyo-cho, Hirosaki, Aomori 036-8561 and [9]Precursory Research for Embryonic Science and Technology, Japan Science and Technology Agency, 4-1-8 Honcho, Kawaguchi, Saitama 332-0012, Japan

Received April 6, 2009; Revised April 1, 2010; Accepted April 14, 2010

ABSTRACT

CeR-2 RNA is one of the newly identified *Caenorhabditis elegans* noncoding RNAs (ncRNAs). The characterization of CeR-2 by RNomic studies has failed to classify it into any known ncRNA family. In this study, we examined the spatiotemporal expression patterns of CeR-2 to gain insight into its function. CeR-2 is expressed in most cells from the early embryo to adult stages. The subcellular localization of this RNA is analogous to that of fibrillarin, a major protein of the nucleolus. It was observed that knockdown of C/D small nucleolar ribonucleoproteins (snoRNPs), but not of H/ACA snoRNPs, resulted in the aberrant nucleolar localization of CeR-2 RNA. A mutant worm with a reduced amount of cellular CeR-2 RNA showed changes in its pre-rRNA processing pattern compared with that of the wild-type strain N2. These results suggest that CeR-2 RNA is a C/D snoRNA involved in the processing of rRNAs.

INTRODUCTION

The ribosome is an essential component of the cell and is deeply involved in the regulation of cell growth, proliferation and differentiation (1–7). Despite its significance, little is known about the biogenesis of the ribosome. In eukaryotes, hundreds of nonribosomal proteins and small nucleolar RNAs (snoRNAs) are involved in ribosome assembly, and it is thought that they are elaborately coordinated to form a functional ribosome in response to cell circumstances (8,9).

Four RNA species are involved in eukaryotic ribosomes: the 18S ribosomal RNA (rRNA), which is a component of the small subunit (40S), and the 5.8S rRNA, 28S rRNA (25S or 28S, depending on the organism) and 5S rRNA, which are components of the large subunit (60S). The 18S, 5.8S and 28S rDNAs are aligned in tandem and cotranscribed by RNA polymerase I in the nucleolus (10). The primary transcripts contain extra sequences designated the 5′ external transcribed spacer (ETS), 3′-ETS, internal transcribed spacer 1 (ITS1) and ITS2, which are removed to produce the mature 18S, 5.8S and 28S rRNAs (11). Studies of rRNA maturation in yeast, frogs and mammals have shown that there are many similarities and differences in the pathways of pre-rRNA processing among species (6,12–15).

Nine snoRNAs (U3, U14, U17/E1/snR30, snR10, U8, U22, MRP, E2 and E3) are related to pre-rRNA processing. U3, U14 and U17/E1/snR30 are evolutionarily conserved snoRNAs that are required for the maturation of 18S rRNA (16–18). MRP snoRNAs are found in a

*To whom correspondence should be addressed. Tel: +81 172 39 3592; Fax +81 172 39 3593; Email: cushida@cc.hirosaki-u.ac.jp
Correspondence may also be addressed to Toshinobu Fujiwara. Tel/Fax: +81 78 803 5728; Email: tosinobu@kobe-u.ac.jp

The authors wish it to be known that, in their opinion, the first two authors should be regarded as joint First Authors.

variety of eukaryotic organisms. According to yeast analyses, this RNA functions in the cleavage of ITS1. However, it is not yet clear whether MRP snoRNA is involved in rRNA maturation in mammals and other organisms too. Similarly, snR10 has been identified in several organisms, but it has not been confirmed that this RNA functions in the cleavage of pre-rRNAs other than in yeast. The remaining snoRNAs, U8, U22, E2 and E3, have only been found in vertebrates to date. U3, U14, U8 and U22 snoRNAs share some features with C/D snoRNAs, and U17/E1/snR30, snR10, E2 and E3 RNAs share features with H/ACA snoRNAs (6,17–23).

Caenorhabditis elegans is a good model to study how various physiological phenomena occur based on the molecular systems in cells. However, little is known about *C. elegans* ribosome biogenesis. Until recently, the cleavage sites of the pre-rRNAs remained unclear (24). U3 is the only snoRNA that probably functions in pre-rRNA cleavage in *C. elegans* (25). Although several RNomic studies have suggested candidates for snR10, U14, U17 and MRP RNA homologs in *C. elegans* (23,26,27), there is no biochemical or genetic evidence that they are involved in pre-rRNA processing. Moreover, it is unclear whether RNAs homologous to U8, U22, E2 or E3 are expressed in *C. elegans*.

In our previous study, we identified 19 novel ncRNA candidates in *C. elegans* (28,29). Seven showed the characteristic secondary structure of the modification-guiding C/D or H/ACA snoRNAs (28). None of the remaining 12 candidates showed marked similarity to any known ncRNA sequence in the database. Here, we show that one of these RNAs, designated CeR-2 RNA and also known as CeN21 or Ce9 (26,30), has several characteristics of a C/D snoRNA and is likely to function in rRNA processing.

MATERIALS AND METHODS

Caenorhabditis elegans strains and culture

Worms were grown and maintained by standard procedures (31). Strain MT16939 containing a *cer-2a* mutant allele (*n5007*), which lacks a region encompassing nts 8 428 510–8 429 125 of chromosome IV, was generated by ethane methyl sulfonate mutagenesis. The *cer-2a* (*n5007*) worms were outcrossed to N2 animals six times before analysis. The *cer-2a* (*n5007*) worms were genotyped by polymerase chain reaction (PCR) using the primers cer-2a-1129 (5′-CCACAAGCTTTCATTTAGAGG-3′) and cer-2a+300 (5′-TTTACAATTGTTGATTACGTTTTTA CCTC-3′). The positions and directions of these primers are shown in Figure 4A.

Plasmids

The plasmid pT7CER2aSP6 was designed to express CeR-2 RNA from a T7 promoter and to express an antisense CeR-2 RNA from an SP6 promoter. The DNA fragments were amplified by nested PCR. The first PCR was performed with a *C. elegans* genomic DNA template and primers CeR2aT7F1 (5′-CGACTCACTATAGTCTTCA GTATGGGTCA-3′) and CeR2aSP6R (5′-AGGTGACA CTATAGTTCAGAATCGGGCTGG-3′), which contain T7 promoter and SP6 promoter sequences (underlined), respectively. The PCR mixture was then used as the template for the second PCR, which was performed with the primers EcoRIT7 (5′-AAAGAATTCTAATACGACT CACTATA-3′) and PstISP6 (5′-AAACTGCAGATTTAG GTGACACTATA-3′). The resulting DNA fragment was digested with *Eco*RI and *Pst*I and ligated into the same sites of pUC19. Clones pT7U18SP6 and pT7U17SP6 were prepared by the same procedures. The primers used for the first PCR were U18(T7)F 5′-CGACTCACTATAGTGGC AGTGATGATCACAAATC-3′, U18(SP6)R 5′-AGGTG ACACTATAGTGGCTCAGCCGGTTTTC-3′, U17(T7)F 5′-CGACTCACTATAGCTCGACATGTGA CTAGCG-3′ and U17(SP6)R 5′-AGGTGACACTATAG ATTTGTAATTTGCATGGTTTG-3′. EcoRIT7 and PstISP6 were used as the second PCR primers. The clone containing part of the rRNA precursor sequence has been described previously (24).

Northern hybridization

Total RNAs from N2 and MT16939 were extracted with TRIzol Reagent or the PureLink RNA Mini Kit (Invitrogen). The RNAs were resolved on formaldehyde-containing 1.0% agarose gel or by 7 M urea/6% polyacrylamide gel electrophoresis and blotted onto Biodyne Plus membrane (Pall Corporation). The blot was hybridized with RNA probes prepared with the DIG RNA Labeling Kit (Roche). The templates for RNA synthesis were amplified by PCR from the clones as described earlier. The probes used for detecting the pre-rRNA intermediates have been described previously (24). Immunoprecipitation with anti-2,2,7-trimethylguanosine (TMG) antibody K121 was based on a previous work (25).

RNA fluorescence *in situ* hybridization of small RNAs and immunofluorescence analysis

Specimens for RNA fluorescence *in situ* hybridization and immunofluorescence analysis were prepared as described previously (32,33). The RNA probes were prepared using the DIG RNA Labeling Kit (SP6/T7) or with MEGAscript/SP6 (Ambion, Inc.) and fluorescein-12-UTP (Enzo Industries, Inc.). The DIG haptens were detected by Cy3-conjugated IgG fraction monoclonal mouse anti-DIG antibody (1:400 dilution; Jackson ImmunoResearch Laboratories, Inc.; lot 59998) or fluorescein-conjugated anti-DIG Fab fragment (1:25 dilution; Roche). Cy3-conjugated Affinipure goat anti-mouse IgG (H+L) antibody (1:400 dilution; Jackson ImmunoResearch Laboratories, Inc.) or Alexa-488-conjugated anti-fluorescein/Oregon Green rabbit polyclonal IgG (1:100 dilution; Molecular Probes, Inc.) was used as the secondary antibody. The signals of the fluorescein-labeled RNA probes were enhanced with Alexa-488-conjugated anti-fluorescein/Oregon Green rabbit antibody and anti-rabbit chicken IgG antibody (1:100; Molecular Probes, Inc.). Fibrillarin (FIB-1) was visualized with the anti-FIB-1 antibody 38F3 (1:400 dilution; EnCor Biotechnology Inc.) and Cy3-conjugated

anti-mouse antibody. The nuclei were stained with 4′,6-diamidino-2-phenylindole dihydrochloride (DAPI). The signals were observed under a light fluorescence microscope (Olympus, BX60) or a confocal laser microscope (Leica, DMI6000, TCS SP5 and Olympus, FV1000D, FV10-ASW).

RNA interference

The template DNAs for *in vitro* transcription were generated by PCR using yk cDNA clones (*nop10* [C25A1.6], yk1472f12; *nop56* [K07C5.4], yk1604e03), which were kind gifts from Dr Yuji Kohara. Oligonucleotides containing the T7 promoter sequence were used as primers (T7ME774FW, 5′-TTTTAATAAT ACGACTCACTATAGCTTCTGCTCTAAAAGCTGC G-3′ and T7ME1250RV, 5′-TAAAGATAATACGACTC ACTATAGTGTGGGAGGTTTTTTCTCTTAG-3′). Sense and antisense RNAs were synthesized using MEGAscript/T7 (Ambion). The resulting RNAs were annealed to generate double-stranded RNAs. The double-stranded RNAs (1 μg/μl) were injected into L4 worms.

RESULTS AND DISCUSSION

Isolation of CeR-2 RNA

CeR-2 RNA is one of the 19 small novel candidate ncRNAs isolated from *C. elegans* (28,29). This RNA is encoded in the intergenic region of chromosome IV. A homologous gene is found on the same chromosome: the former is designated *cer-2a* and the latter is designated *cer-2b* (chromosome IV, nts 4 880 726–4 880 851, complement). A BLAST search showed that the genomes of nematodes closely related to *C. elegans*, *C. briggsae* (CB3; 2006), *C. brenneri* (6.0.1 contigs), *C. remanei* (15.0.1 supercontigs) and *C. japonica* (3.0.2 supercontigs), have two, six, three and two homologs of CeR-2, respectively, but no similar sequence was found in any other organism. Figure 1A shows the sequence alignment of the CeR-2 RNA gene with its homologs, constructed using Align X of the software package Vector NTI ver. 9 (Invitrogen). There are two highly conserved sequences: one corresponds to the sequence of CeR-2 RNA itself and the other is located ~30–40-bp upstream from the CeR-2-RNA-coding region. The upstream sequence (−32 to −69 in Figure 1A) is similar to the proximal sequence element, which functions as a promoter in U snRNA genes (34–37). This suggests that CeR-2 RNA is transcribed by RNA polymerase II and has a TMG cap at its 5′ end. To examine this possibility, we performed immunoprecipitation with the anti-TMG antibody K121 against the total RNAs extracted from mixed-stage worms. The anti-TMG-precipitated RNAs were then subjected to Northern blot analysis (Figure 1B). As a control for immunoprecipitation specificity, U6 snRNA, which does not have a TMG cap (25), was also monitored by Northern blot analysis. Most of the CeR-2 RNA was detected in the K121 precipitate, whereas the majority of the U6 snRNA was detected in the supernatant. This indicates that most CeR-2 RNAs in the cell have a TMG cap at their 5′ ends, like other *C. elegans* small RNAs, such as the U snRNAs, SL RNAs (38) and U3 snoRNA (25).

Spatiotemporal expression patterns and subcellular localization of CeR-2 RNA

We examined the spatiotemporal expression patterns and subcellular localization of CeR-2 RNA by *in situ* hybridization. As shown in Figure 2A, CeR-2 is expressed in most cells in L1 larvae and it continues to be expressed until adulthood in both the somatic and germline cells. Consistently, Northern hybridization of total RNA revealed that CeR-2 is expressed constitutively during the four larval stages and the adult stage (Figure 2B).

To determine the subcellular localization of CeR-2, we inspected the large intestinal nucleus (Figure 2C). Foci of CeR-2 RNA were detected inside the nucleus and completely overlapped with the signals for FIB-1 (Figure 2C). This indicates that CeR-2 RNA localizes in the nucleolus. Thus, CeR-2 RNA shares the most characteristic feature of the snoRNAs that function in pre-rRNA processing or rRNA modification.

Changes in the nucleolar localization of CeR-2 RNA by knockdown of the C/D snoRNP gene

There are two major snoRNA families, the C/D snoRNA and H/ACA snoRNA families. Four core proteins interact specifically with the RNAs of each family: fibrillarin/NOP1, NOP56, NOP58 and a 15.5-kDa protein with C/D snoRNAs, and dyskerin/NAP57, NHP2, NOP10 and GAR1 with H/ACA snoRNAs (39). We expected that some of these proteins would interact with CeR-2 RNA and contribute to its function and nucleolar localization. Therefore, we knocked down the expression of the *C. elegans* C/D snoRNP gene *nop56* (K07C5.4) and the H/ACA snoRNP gene *nop10* (C25A1.6). The effects of RNA interference (RNAi) were assayed by *in situ* hybridization and immunofluorescence.

As expected, knockdown of *nop56*, which encodes a C/D snoRNP-specific protein, markedly reduced the signals of CeR-2 RNA and FIB-1 (Figure 3A). In several cells of the *nop56* (*RNAi*) worm, both signals were observed in a limited region at the periphery of the nucleolus (Figure 3A and B, arrows). U18 snoRNA, a typical C/D snoRNA, was used as an internal control to monitor the knockdown effect of *nop56*. The level of nucleolar localization was reduced by the reduction of Nop56 but not by the reduction of Nop10. The effect of *nop10* knockdown was confirmed by the reduction of the U17 H/ACA-type snoRNA (Figure 3C). It is likely that CeR-2 RNA is a member of the C/D snoRNA family and functions in the nucleolus together with C/D snoRNPs. A recent study based on a microarray indicated that the knockdown of *nop58* or *snu13* leads to a severe reduction in CeR-2 RNA (CeN21 RNA in refs. 26 and 40). This also supports our prediction that CeR-2 RNA is a C/D snoRNA.

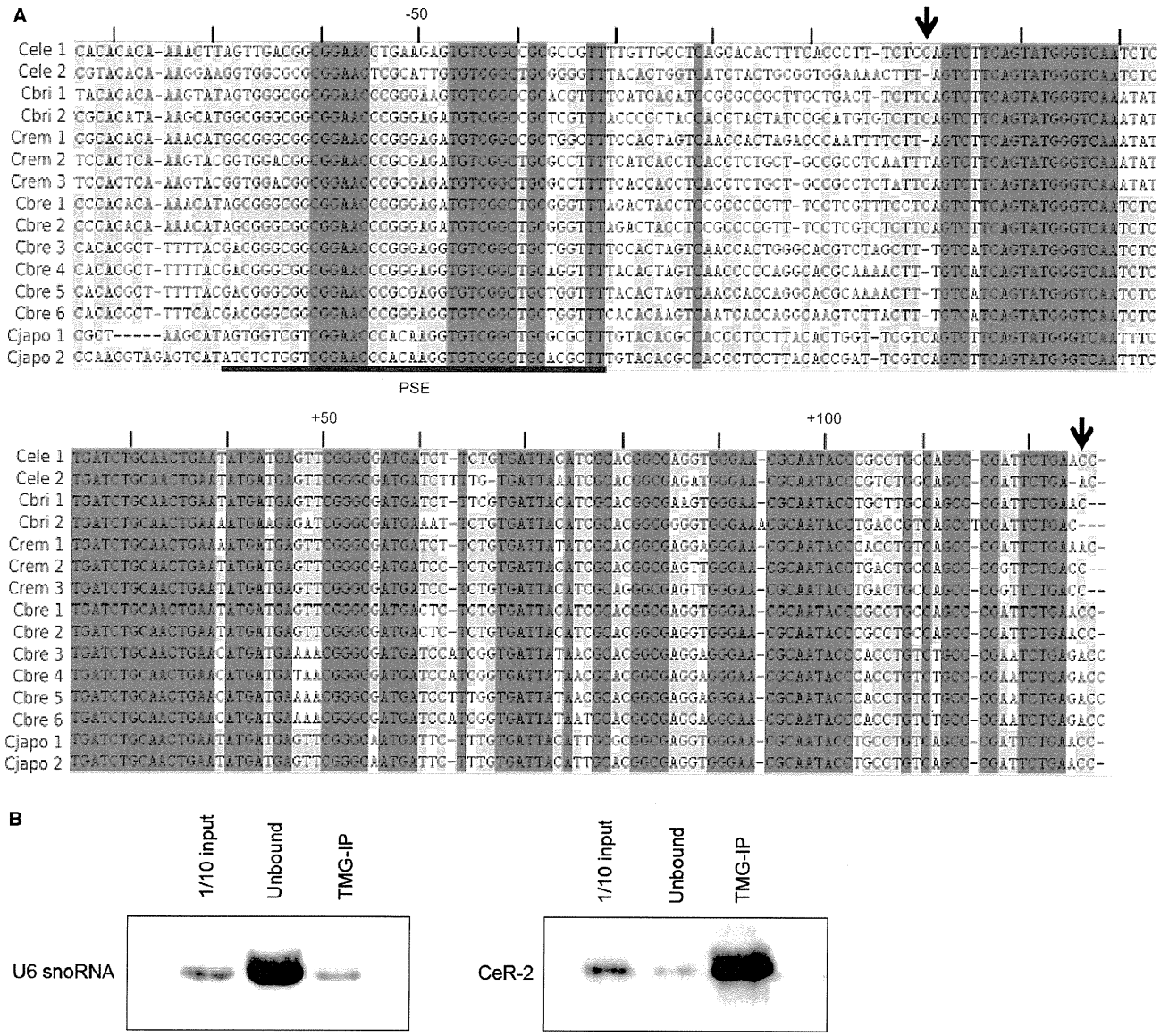

Figure 1. Sequence alignment of CeR-2 RNA genes. (**A**) Sequence alignment of *cer-2a* and its homologs. The sequences conserved among all 15 homologs are shaded in dark gray. Partially conserved sequences are shaded in light gray. Cele1, *cer-2a*; Cele2, *cer-2b*; Cbri1, *C. briggsae* homolog of *cer-2a*; Cbri2, *C. briggsae* homolog of *cer-2b*; Crem1-3, three homologs found in *C. remanei*; Cbre1-6, six homologs found in *C. brenneri*; Cjapo1 and Cjapo2, two homologs found in *C. japonica*. The putative 5′- and 3′-terminal nucleotides of the RNA-coding region in *cer-2a* are indicated by arrows. (**B**) *Caenorhabditis elegans* TMG-capped RNA was precipitated with the anti-TMG antibody K121. Northern hybridization was performed with antisense probes of CeR-2 RNA and U6 snRNA against the precipitate (TMG-IP) and the supernatant (Unbound). A 1/10 amount of total RNA input was also separated on the same denaturing gel and blotted onto a nylon membrane (1/10 input).

A mutant lacking *cer-2a* shows an altered accumulation pattern of pre-rRNAs

To determine the function of CeR-2 RNA, we produced a mutant strain lacking *cer-2a* and designated it MT16939. This deletion mutant of *cer-2a* (*n5007*) lacks a 618-bp sequence on chromosome IV (Figure 4A and B). Northern blot analysis indicated that CeR-2 RNA was reduced by about half to one-third in *cer-2a* mutants compared with that in wild-type N2 worms (Figure 4C). The remaining CeR-2 RNA signal on Northern blots originated from *cer-2b*, a homolog of *cer-2a*, with a 98% identical sequence. The homozygous mutant of *cer-2a* showed a slow growth phenotype and abnormal fertilization, especially in old adults. We tried to generate a mutant of *cer-2b*, but were unsuccessful.

Because CeR-2 RNA exhibits the characteristics of a box C/D-type snoRNA, it was expected that CeR-2 RNA would function in guiding the 2′-*O*-methylation of

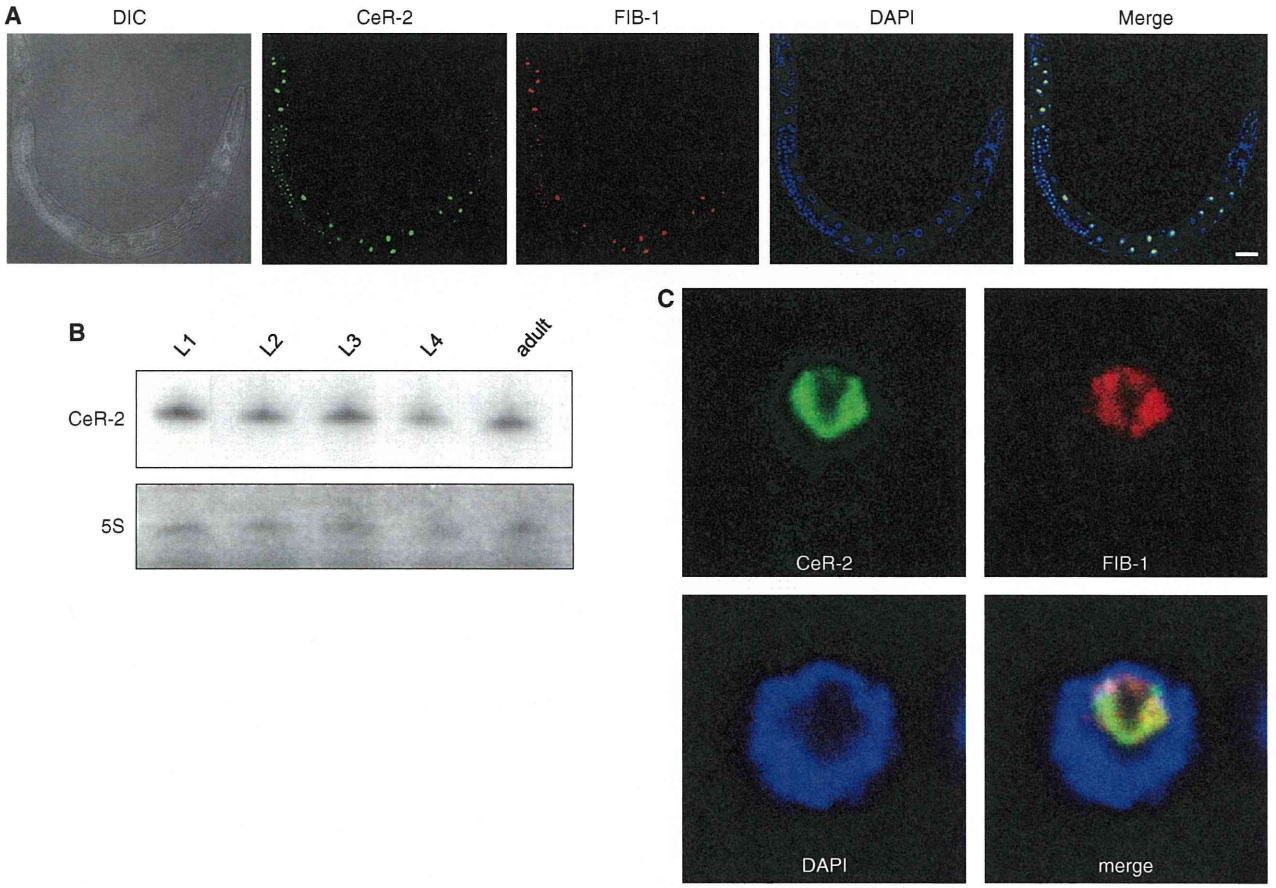

Figure 2. Spatiotemporal expression patterns of CeR-2 RNA. (**A**) CeR-2 RNA was detected by *in situ* hybridization (CeR-2, green). FIB-1 was costained with an anti-FIB antibody (FIB-1, red). DIC, Nomarski differential interference contrast microscopic image; DAPI, DNA visualized with DAPI staining; Merge, merged images of CeR-2, FIB-1, and DAPI. Scale bar, 5 μm. (**B**) Northern hybridization of CeR-2 RNA against total RNAs prepared from the larvae of each stage (L1 to L4) and adults. The 5S rRNA band on the blot was detected with methylene blue staining. (**C**) CeR-2 RNA foci in the nucleus overlapped with FIB-1 foci. The stained images of an intestinal nucleus are magnified. CeR-2 RNA (green) and FIB-1 (red) were stained with DAPI.

rRNAs and/or in processing pre-rRNAs (1–6,41,42). One important structural feature of modification guiding C/D snoRNAs is that the region upstream from the D or D′ box encompasses 10–21 bp complementary to the target rRNA around the modification site. When the duplex is <9 bp or contains substantial AU or GU pairs, methylation becomes less efficient (42). Therefore, searching for a complementary sequence to an rRNA sequence longer than 10 bp is one way to assess the function of a C/D snoRNA in guiding the 2′-*O*-methylation of rRNA. We searched for a complementary sequence between CeR-2 RNA and *C. elegans* rRNAs that was longer than 10 bp. However, no such continuous sequences were found, which reduced our expectation that CeR-2 RNA functions in guiding the modification of rRNAs.

An outline of *C. elegans* rRNA processing was established in a previous study (Figure 5A) (24). In N2 worms, five pre-rRNA processing intermediates were detected and designated a, b, c, c′ and d. We designed four probes (probes 3, 4, 5 and 6), with reference to the study of Saijou *et al.* (24), to detect each intermediate. Figure 5B shows the results of Northern hybridization of RNA extracts from N2 (wild-type) worms and MT16939 (*cer-2a* [*n5007*]) worms with these probes. Intermediate c′ accumulated more in MT16939 than in N2, as shown in the results for probes 4, 5 and 6 (Figure 5B, lanes 4, 6 and 8, respectively). The accumulation of c′ indicates that the efficiency of processing the large subunit rRNA precursor into 5.8S and 26S rRNAs was reduced in the mutant after the cleavage of the pre-rRNA in ITS1. The results for probe 3 showed reductions in intermediates b and/or d in the mutant (Figure 5B, lanes 1 and 2, respectively). Intermediate d, detected with probe 4, did not differ significantly between N2 and MT16939 (Figure 5B, lanes 3 and 4, respectively), which indicates that intermediate b, which is a precursor of 18S rRNA, was reduced in the mutant. Therefore, MT16939 exhibited changes in the accumulation patterns of the rRNA precursors. This suggests that CeR-2 RNA is involved in the processing of pre-rRNAs, although it is

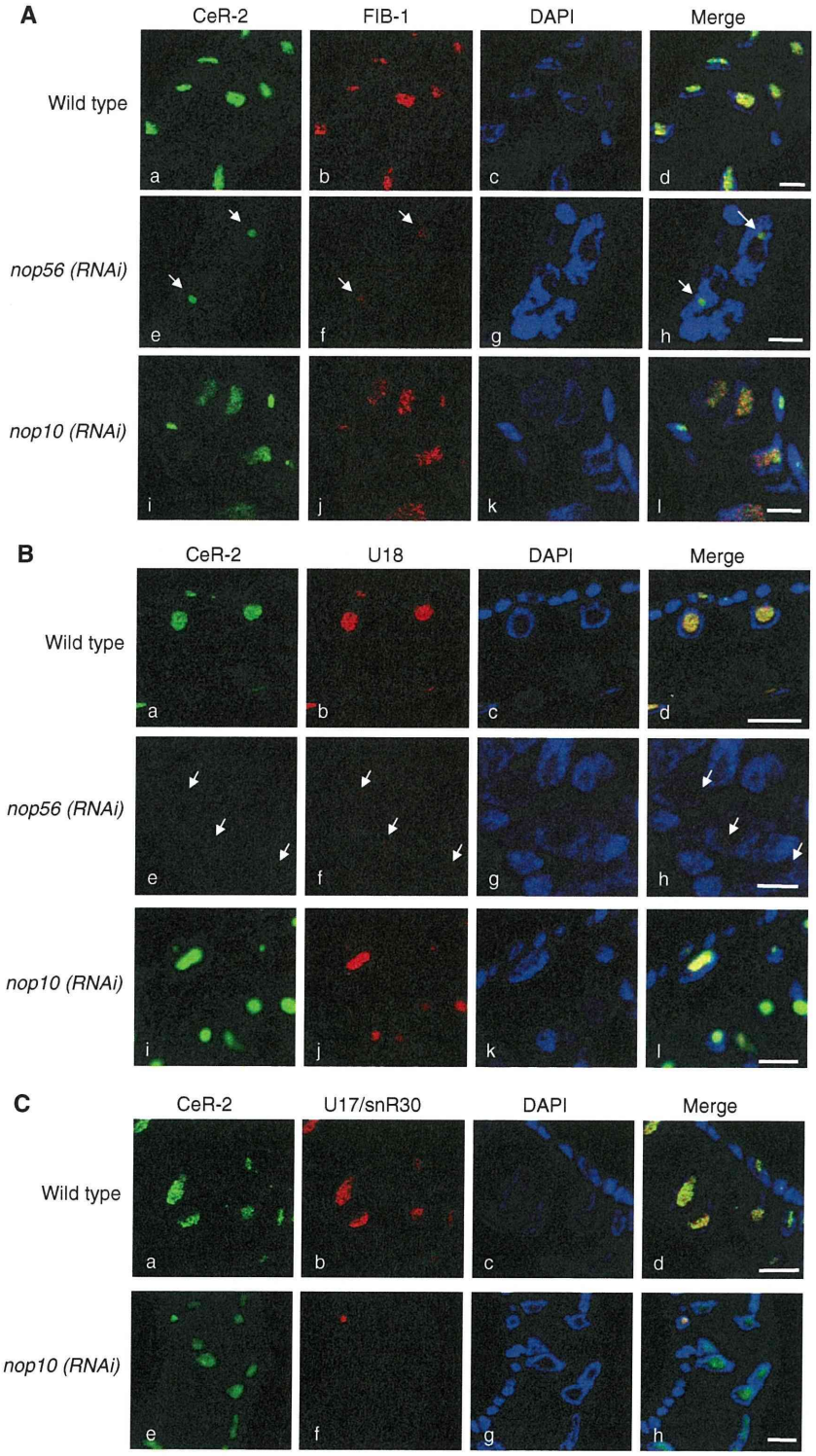

Figure 3. Knockdown of *nop56* reduced the nucleolar localization of CeR-2 RNA. Each nucleolar factor was observed by *in situ* hybridization or immunofluorescence analysis. The white arrows indicate the accumulation of CeR-2 RNA, FIB-1 or U18 snoRNA in the foci, which newly appeared in the nucleoplasm after the knockdown of *nop56*. Scale bars, 5 μm. (**A**) Costaining of CeR-2 RNA (green, panels a, e and i) and FIB-1 (red, panels b, f and j) in *nop56* (RNAi) and *nop10* (RNAi) worms. (**B**) Costaining of CeR-2 RNA (green, panels a, e and i) and U18 C/D snoRNA (red, panels b, f and j) in *nop56* (RNAi) worms and *nop10* (RNAi) worms. (**C**) Costaining of CeR-2 RNA (green, panels a, e and i) and U17/snR30 H/ACA snoRNA (red, panels b, f and j) in *nop10* (RNAi) worms. Panels c, g and k, DAPI staining; panels d, h and l, merged images.

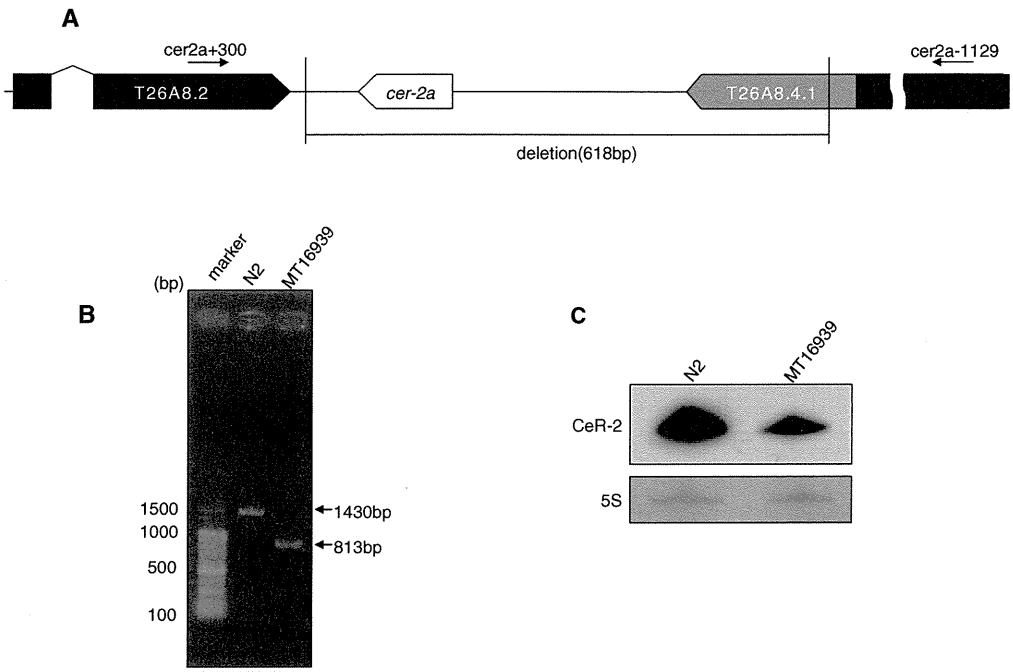

Figure 4. CeR-2 RNA expression in MT16939. (**A**) Genomic map around *cer-2a* of MT16939 on chromosome IV. The primers cer-2a-1129 and cer-2a+300 refer to the PCR primers used for genotyping N2 and MT16939. There are two putative protein genes, T26A8.2 and T26A8.4.1, adjacent to *cer-2a*. (**B**) Genotyping of N2 and MT16939 worms by single-worm PCR. Marker, 100-bp DNA ladder; N2, PCR product amplified from the genomes of N2 worms; MT16939, PCR product amplified from the genomes of MT16939 worms. The PCR products are indicated by arrows with their putative lengths (bp). (**C**) Northern hybridization of total RNAs from N2 and MT16939 with the CeR-2 RNA antisense probe. The 5S rRNA band on the blot, stained with methylene blue, is shown subsequently.

still possible that CeR-2 RNA guides the modification of rRNAs.

Because MT16939 lacks a part of the 3′ untranslated region (UTR) of the gene upstream from *cer-2a* (T26A8.4.1), it is possible that T26A8.4.1 affects the processing of rRNAs. The homozygous mutation of T26A8.4.1 is lethal and it is therefore difficult to analyze the pre-rRNA patterns. We tried to detect pre-rRNAs in worms in which T26A8.4.1 was knocked down. Although no obvious changes in the pre-rRNA pattern were observed, we cannot completely rule out the possibility that T26A8.4.1 is relevant to rRNA processing.

U8 and U22 snoRNAs are C/D-type snoRNAs related to the cleavage of rRNA processing. They have been identified only in vertebrates and their homologs have not been found in invertebrates to date. Some features of CeR-2 RNA shown here revealed similarity to those of U8 snoRNAs: both RNAs are TMG-capped, have features of C/D snoRNAs, and are involved in the cleavage of ITS2. In addition, the 5′-terminal sequence of CeR-2 RNA has the potential to base pair with that of *C. elegans* 26S rRNA, as U8 snoRNA base pairs with the 5′ terminus of 28S rRNA (Figure 6). There is a sequence similar to the conserved LSm binding motif of U8 snoRNA in the second stem-loop (Figure 6). Thus, CeR-2 RNA is an excellent candidate to be a U8 ortholog.

ACKNOWLEDGEMENTS

The authors thank Dr Robert Horvitz and Dr Ezequiel Alvarez-Saavedra at the Department of Biology, Massachusetts Institute of Technology, Cambridge, for isolating the *cer-2a* (*n5007*) worm. They also thank Dr Katsuya Yamada at the School of Medicine, Hirosaki University, and the staff of the Gene Research Center of Hirosaki University for allowing us the use of their facilities.

FUNDING

Grant-in Aid for Scientific Research (C) 18570157 to C.U. from the Ministry of Education, Science, Sports and Culture (MEXT), Japan; a grant from the Functional RNA Project to C.U. from the Ministry of Economy, Trade and Industry; NEDO, Special Coordination Funds for Promoting Science and Technology; the Creation of Innovation Centers for Advanced Interdisciplinary Research Areas (Innovative Bioproduction Kobe) to T.F. from MEXT, Japan; and the 21st COE Program of Iwate University to Y.H.

Conflict of interest statement. None declared.

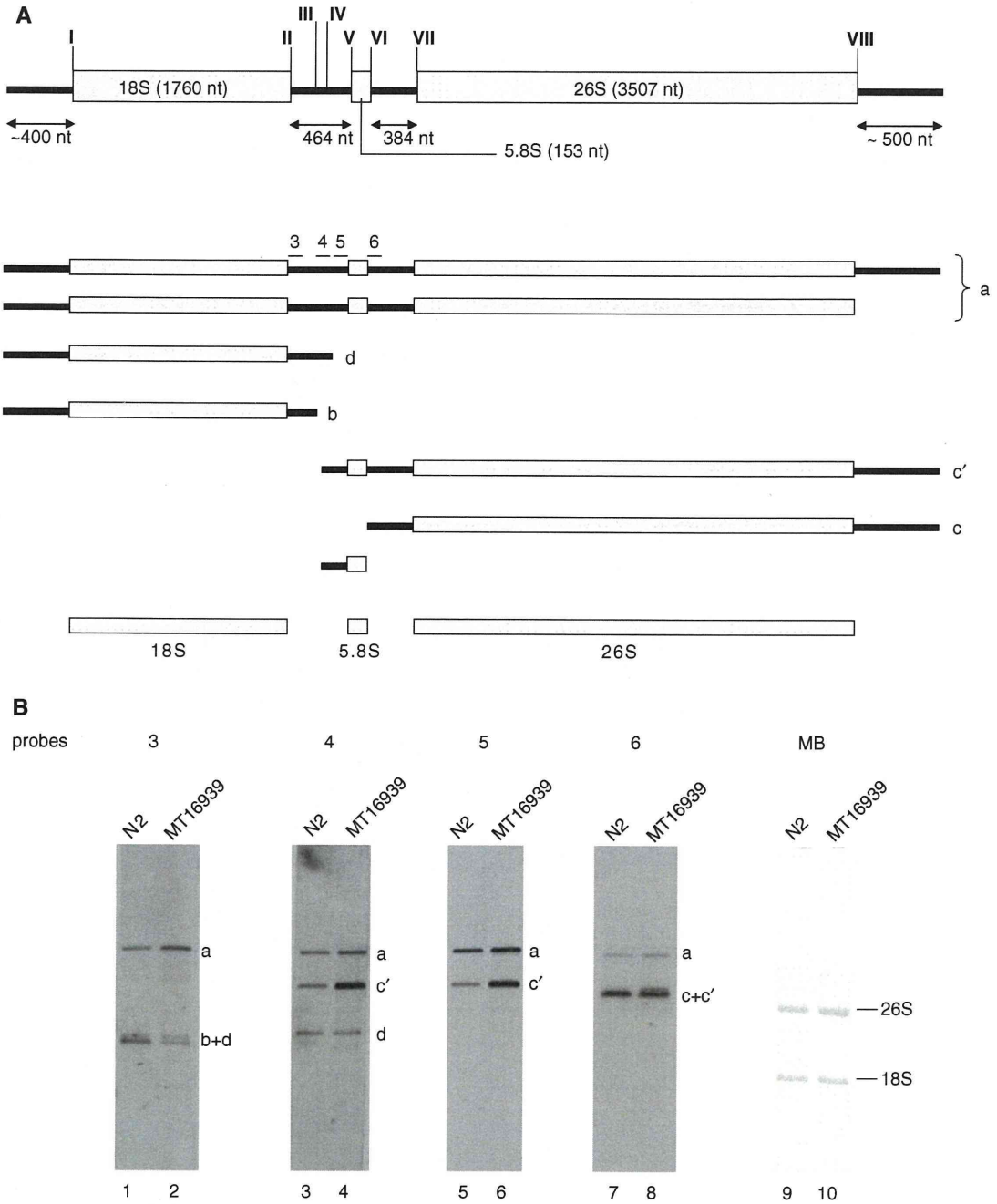

Figure 5. pre-rRNAs in MT16939. (**A**) Schematic representation of pre-rRNA processing pattern. Probes 3, 4, 5, and 6 used for the hybridization are indicated by bars above intermediate **a**. The cleavage sites (I–VIII) are indicated along the precursor **a** with reference to the study of Saijou *et al.* (24). The length of the rDNA is based on nucleotide data for GenBank accession number X03680. (**B**) Comparison of the pre-rRNA patterns of N2 and MT16939. Northern hybridization of the RNAs from N2 (lanes 1, 3, 5 and 7) and MT16939 (lanes 2, 4, 6 and 8) with each probe. Intermediates a, b, c, c′ and d indicate the pre-rRNAs shown in Figure 5A. The membrane was stained with methylene blue (lanes 9 and 10, MB), and the 26S and 18S rRNA bands are shown.

REFERENCES

1. Venema,J. and Tollervey,D. (1999) Ribosome synthesis in *Saccharomyces cerevisiae*. *Annu. Rev. Genet.*, **33**, 261–311.
2. Fromont-Racine,M., Senger,B., Saveanu,C. and Fasiolo,F. (2003) Ribosome assembly in eukaryotes. *Gene*, **313**, 17–42.
3. Granneman,S. and Baserga,S.J. (2004) Ribosome biogenesis: of knobs and RNA processing. *Exp. Cell Res.*, **296**, 43–50.
4. Hage,A.E. and Tollervey,D. (2004) Why is ribosome assembly so much more complicated in eukaryotes than bacteria? *RNA Biol.*, **1**, 10–15.
5. Dinman,J. (2009) The eukaryotic ribosome: current status and challenges. *J. Biol. Chem.*, **284**, 11761–11765.

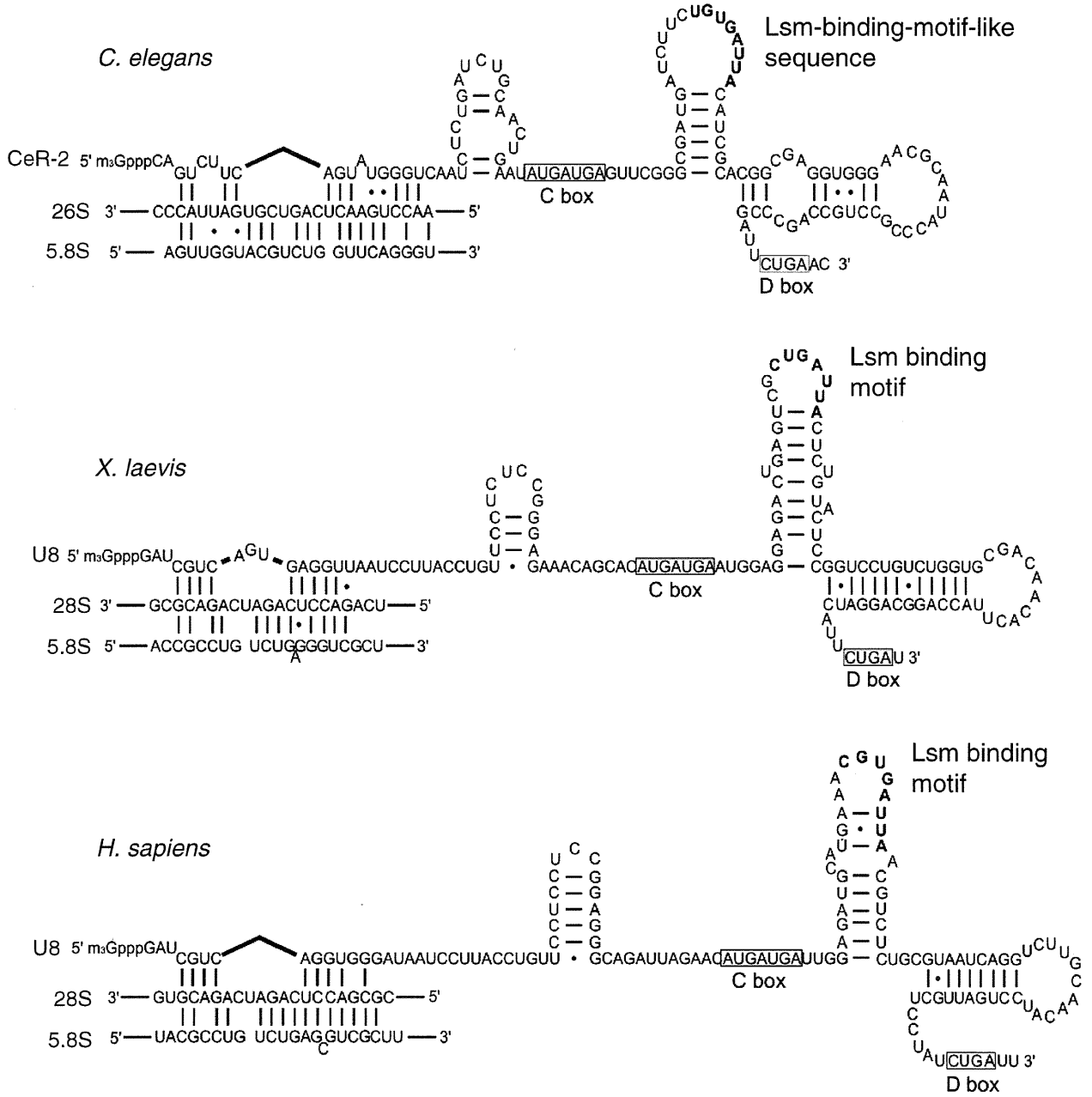

Figure 6. Comparison of the predicted secondary structures of CeR-2 RNA and vertebrate U8 snoRNAs. Potential base pairing between the 5′ region of CeR-2 RNA and the 5′ region of 26S rRNA is shown and compared with that between U8 snoRNA and 28S rRNA of *Xenopus laevis* and *Homo sapiens* (20,43). There are three stem-loops in the remaining 3′ part of CeR-2 RNA, which appear in the secondary structure of U8 snoRNAs in similar regions: one upstream from the C-box and the other two between the C-box and the D-box (open rectangles). The LSm binding motif is a conserved octameric sequence located in the loop of the second stem-loop in U8 snoRNAs (44). Similar sequences (six of the conserved eight nucleotides, LSm-binding-motif-like sequence) are also found in the loop of the second stem-loop of CeR-2 RNA (bold letters).

6. Gerbi,S.A., Borovjagin,A.V., Ezrokhi,M. and Lange,T.S. (2001) Ribosome biogenesis: role of small nucleolar RNA in maturation of eukaryotic rRNA. *The Ribosome, Cold Spring Harbor Symposia on Quantitative Biology*, Vol. LXVI. Cold Spring Harbor Laboratory Press, Cold Spring Harbor, NY, pp. 575–590.
7. Henras,A.K., Soudet,J., Gerus,M., Lebaron,S., Caizergues-Ferrer,M., Mougin,A. and Henry,Y. (2008) The post-transcriptional steps of eukaryotic ribosome biogenesis. *Cell. Mol. Life Sci.*, **65**, 2334–2359.
8. Yewdell,J.W. and Nicchitta,C.V. (2006) The DRiP hypothesis decennial: support, controversy, refinement and extension. *Trends Immunol.*, **27**, 368–373.
9. Kelleher,R.J. III and Bear,M.F. (2008) The autistic neuron: troubled translation? *Cell*, **135**, 401–406.

10. Mougey,E.B., O'Reilly,M., Osheim,Y., Miller,O.L. Jr, Beyer,A. and Sollner-Webb,B. (1993) The terminal balls characteristic of eukaryotic rRNA transcription units in chromatin spreads are rRNA processing complexes. *Genes Dev.*, **7**, 1609–1619.
11. Winicov,I. (1976) Alternate temporal order in ribosomal RNA maturation. *J. Mol. Biol.*, **100**, 141–155.
12. Dabeva,M.D., Dudov,K.P., Hadjiolov,A.A., Emanuilov,I. and Todorov,B.N. (1976) Intranuclear maturation pathways of rat liver ribosomal ribonucleic acids. *Biochem. J.*, **160**, 495–503.
13. Loening,U.E., Jones,K.W. and Birnstiel,M.L. (1969) Properties of the ribosomal RNA precursor in *Xenopus laevis*; comparison to the precursor in mammals and in plants. *J. Mol. Biol.*, **45**, 353–366.
14. Udem,S.A. and Warner,J.R. (1973) The cytoplasmic maturation of a ribosomal precursor ribonucleic acid in yeast. *J. Biol. Chem.*, **248**, 1412–1416.
15. Borovjagin,A.V. and Gerbi,S.A. (1999) U3 small nucleolar RNA is essential for cleavage at sites 1, 2 and 3 in pre-rRNA and determines which rRNA processing pathway is taken in *Xenopus* oocytes. *J. Mol. Biol.*, **286**, 1347–1363.
16. Atzorn,V., Fragapane,P. and Kiss,T. (2004) U17/snR30 is a ubiquitous snoRNA with two conserved sequence motifs essential for 18S rRNA production. *Mol. Cell. Biol.*, **24**, 1769–1778.
17. Enright,C.A., Maxwell,E.S., Eliceiri,G.L. and Sollner-Webb,B. (1996) 5′ETS rRNA processing facilitated by four small RNAs: U14, E3, U17, and U3. *RNA*, **2**, 1094–1099.
18. Mishra,R.K. and Eliceiri,G.L. (1997) Three small nucleolar RNAs that are involved in ribosomal RNA precursor processing. *Proc. Natl Acad. Sci. USA*, **94**, 4972–4977.
19. Peculis,B.A. and Steitz,J.A. (1993) Disruption of U8 nucleolar snRNA inhibits 5.8S and 28S rRNA processing in the *Xenopus* oocyte. *Cell*, **73**, 1233–1245.
20. Peculis,B.A. (1997) The sequence of the 5′ end of the U8 small nucleolar RNA is critical for 5.8S and 28S rRNA maturation. *Mol. Cell. Biol.*, **17**, 3702–3713.
21. Tycowski,K.T., Shu,M.D. and Steitz,J.A. (1994) Requirement for intron-encoded U22 small nucleolar RNA in 18S ribosomal RNA maturation. *Science*, **266**, 1558–1561.
22. Tycowski,K.T., Kolev,N.G., Conrad,N.K., Fok,V. and Steitz,J.A. (2006) The ever-growing world of small nuclear ribonucleoproteins. In Gesteland,R.F., Cech,T.R. and Atkins,J.F. (eds), *The RNA World*, 3rd edn. Cold Spring Harbor Laboratory Press, Cold Spring Harbor, NY, pp. 327–368.
23. Huang,Z.P., Chen,C.J., Zhou,H., Li,B.B. and Qu,L.H. (2007) A combined computational and experimental analysis of two families of snoRNA genes from *Caenorhabditis elegans*, revealing the expression and evolution pattern of snoRNAs in nematodes. *Genomics*, **89**, 490–501.
24. Saijou,E., Fujiwara,T., Suzaki,T., Inoue,K. and Sakamoto,H. (2004) RBD-1, a nucleolar RNA-binding protein, is essential for *Caenorhabditis elegans* early development through 18S ribosomal RNA processing. *Nucleic Acids Res.*, **32**, 1028–1036.
25. Sasano,Y., Hokii,Y., Inoue,K., Sakamoto,H., Ushida,C. and Fujiwara,T. (2008) Distribution of U3 small nucleolar RNA and fibrillarin during early embryogenesis in *Caenorhabditis elegans*. *Biochimie*, **90**, 898–907.
26. Deng,W., Zhu,X., Skogerbø,G., Zhao,Y., Fu,Z., Wang,Y., He,H., Cai,L., Sun,H., Liu,C. *et al.* (2006) Organization of the *Caenorhabditis elegans* small non-coding transcriptome: genomic features, biogenesis, and expression. *Genome Res.*, **16**, 20–29.
27. Lopez,M.D., Rosenblad,M.A. and Samuelsson,T. (2009) Conserved and variable domains of RNase MRP RNA. *RNA Biol.*, **6**, 208–220.
28. Wachi,M., Ogawa,T., Yokoyama,K., Hokii,Y., Shimoyama,M., Muto,A. and Ushida,C. (2004) Isolation of eight novel *Caenorhabditis elegans* small RNAs. *Gene*, **335**, 47–56.
29. Hokii,Y., Kubo,A., Ogasawara,T., Nogi,Y., Taneda,A., Arai,R., Muto,A. and Ushida,C. (2006) Twelve novel *C. elegans* RNA candidates isolated by two-dimensional polyacrylamide gel electrophoresis. *Gene*, **365**, 83–87.
30. Zemann,A., op de Bekke,A., Kiefmann,M., Brosius,J. and Schmitz,J. (2006) Evolution of small nucleolar RNAs in nematodes. *Nucleic Acids Res.*, **34**, 2676–2685.
31. Brenner,S. (1974) The genetics of *Caenorhabditis elegans*. *Genetics*, **77**, 71–94.
32. Tabara,H., Motohashi,T. and Kohara,Y. (1996) A multi-well version of *in situ* hybridization on whole mount embryos of *Caenorhabditis elegans*. *Nucleic Acids Res.*, **24**, 2119–2124.
33. Mitani,S., Du,H., Hall,D.H., Driscoll,M. and Chalfie,M. (1993) Combinatorial control of touch receptor neuron expression in *Caenorhabditis elegans*. *Development*, **119**, 773–783.
34. Savino,R., Hitti,Y. and Gerbi,S.A. (1992) Genes for *Xenopus laevis* U3 small nuclear RNA. *Nucleic Acids Res.*, **20**, 5435–5442.
35. Peculis,B.A., DeGregorio,S. and McDowell,K. (2001) The U8 snoRNA gene family: identification and characterization of distinct, functional U8 genes in Xenopus. *Gene*, **274**, 83–92.
36. Thomas,J., Lea,K., Zucker-Aprison,E. and Blumenthal,T. (1990) The spliceosomal snRNAs of *Caenorhabditis elegans*. *Nucleic Acids Res.*, **18**, 2633–2642.
37. Li,T., He,H., Wang,Y., Zheng,H., Skogerbø,G. and Cheng,R. (2008) *In vivo* analysis of *Caenorhabditis elegans* noncoding RNA promoter motifs. *BMC Mol. Biol.*, **9**, 71.
38. Thomas,J.D., Conrad,R.C. and Blumenthal,T. (1988) The *C. elegans trans*-spliced leader RNA is bound to Sm and has trimethylguanosine cap. *Cell*, **54**, 533–539.
39. Reichow,S.L., Hamma,T., Ferré-D'Amaré,A.R. and Varani,G. (2007) The structure and function of small nucleolar ribonucleoproteins. *Nucleic Acids Res.*, **35**, 1452–1464.
40. Aftab,M.N., He,H., Skogerbø,G. and Chen,R. (2008) Microarray analysis of ncRNA expression patterns in *Caenorhabditis elegans* after RNAi against snoRNA associated proteins. *BMC Genomics*, **9**, 278.
41. Matera,A.G., Terns,R.M. and Terns,M. (2007) Non-coding RNAs: lessons from the small nuclear and small nucleolar RNAs. *Nat. Rev. Mol. Cell Biol.*, **8**, 209–220.
42. Cavaillé,J. and Bachellerie,J.P. (1998) SnoRNA-guided ribose methylation of rRNA: structural features of the guide RNA duplex influencing the extent of the reaction. *Nucleic Acids Res.*, **26**, 1576–1587.
43. Peculis,B.A. and Steitz,J.A. (1994) Sequence and structural elements critical for U8 snRNP function in *Xenopus* oocytes are evolutionarily conserved. *Genes Dev.*, **8**, 2241–2255.
44. Tomasevic,N. and Peculis,B.A. (2002) *Xenopus* LSm proteins bind U8 snoRNA via an internal evolutionarily conserved octamer sequence. *Mol. Cell Biol.*, **22**, 4101–4112.

Analytical Biochemistry 417 (2011) 182–187

Contents lists available at ScienceDirect

Analytical Biochemistry

journal homepage: www.elsevier.com/locate/yabio

Amplification of agonist stimulation of human G-protein-coupled receptor signaling in yeast

Nobuo Fukuda [a], Jun Ishii [b], Misato Kaishima [a], Akihiko Kondo [a,*]

[a] Department of Chemical Science and Engineering, Graduate School of Engineering, Kobe University, Nada-ku, Kobe 657-8501, Japan
[b] Organization of Advanced Science and Technology, Kobe University, Nada-ku, Kobe 657-8501, Japan

ARTICLE INFO

Article history:
Received 11 March 2011
Received in revised form 27 May 2011
Accepted 6 June 2011
Available online 13 June 2011

Keywords:
Yeast
GPCR
G-protein signaling
Gβ subunit
Feedback signal activation

ABSTRACT

G-protein-coupled receptors (GPCRs) are considered as important targets for drug discovery. The yeast *Saccharomyces cerevisiae* is an attractive host for high-throughput screening of agonistic ligands for human GPCRs because it can simplify the complicated signaling pathways that are present in mammalian cell lines. Unfortunately, many human GPCRs induce only partial signal activation in yeast cells depending on their coupling efficiency with yeast G-proteins. This problem often results in unsatisfactory detection sensitivity, thereby resulting in a limitation to yeast-based detection systems. Here we introduce a new highly sensitive detection method that provides robust agonist detection of human GPCRs. Our strategy is designed to invoke feedback activation of signals within yeast G-protein signaling pathways. Briefly, agonist stimulation of human GPCRs triggers expression of an artificial signal activator that amplifies signaling. We chose human somatostatin receptor subtype 5 (hSSTR5) as a model of a human GPCR. Investigation of the response of hSSTR5-expressing yeast to various concentrations of somatostatin demonstrated that feedback activation of the signal can successfully improve the detection limit and the maximum level of signaling. This novel approach will enhance the usefulness of yeast-based screening of agonistic ligands for a variety of human GPCRs.

G-protein-coupled receptors (GPCRs)[1] constitute the largest family of transmembrane proteins and play an important part in signal transduction by converting extracellular stimuli into intracellular signals. Currently, more than 30% of marketed medicines act on GPCRs, which are still considered as attractive targets for new medicines [1]. To develop new medicines, it is necessary to evaluate a lot of candidates due to the low frequency of discovery of lead compounds. Therefore, high-throughput screening (HTS) of active compounds has become an integral technology in pharmaceutical laboratories [2].

The budding yeast *Saccharomyces cerevisiae* is an attractive host cell system for identification of agonistic ligands that can modulate the functions of human GPCRs because the mechanisms of G-protein signaling are highly conserved among a diverse range of eukaryotes from yeast to mammals. The yeast system, which is composed of an uncompetitive and monopolistic G-protein signaling pathway (the pheromone signaling pathway) [3], is more simple than the complicated G-protein signaling that occurs in mammalian cell lines. It has also been reported that a variety of human GPCRs can successfully activate the yeast signaling pathway when expressed in yeast cells. These receptors respond to binding of their agonists and transmit signals via coupling with the endogenous yeast G-protein, which is a heterotrimer consisting of Gα, Gβ, and Gγ subunits [4]. Whereas a heterotrimeric Gαβγ complex is formed in the unstimulated state (without agonistic ligand), binding of agonist to the receptor induces dissociation of the heterotrimeric G-protein into monomeric Gα and a Gβγ complex, which is accompanied by the exchange of GDP for GTP on the Gα subunit (Fig. 1A). In yeast, the dissociated Gβγ complex activates intracellular effector proteins that stimulate the mitogen-activated protein kinase (MAPK) cascade, resulting in changes in cell behavior (Fig. 1A).

Because cellular responses to MAPK activation, including changes in gene transcription, can be used to detect GPCR agonist-induced signaling, several reporter gene assays have been adopted to assay the signaling stimulated by GPCR agonists in yeast systems (Fig. 1A). Although the *HIS3* and *lacZ* genes [5,6] are conventional reporter genes that are used for auxotrophic screening and colorimetric evaluation, respectively, it was recently reported that a *GFP* fluorescent reporter gene can be used for quantitative HTS using flow cytometry [7–9]. One problem with using

* Corresponding author. Fax: +81 78 803 6196.
E-mail address: akondo@kobe-u.ac.jp (A. Kondo).

[1] *Abbreviations used:* GPCR, G-protein-coupled receptor; HTS, high-throughput screening; MAPK, mitogen-activated protein kinase; hSSTR5, human somatostatin receptor subtype 5; PCR, polymerase chain reaction; EGFP, enhanced green fluorescent protein; SST, somatostatin.

0003-2697/$ - see front matter © 2011 Elsevier Inc. All rights reserved.
doi:10.1016/j.ab.2011.06.006

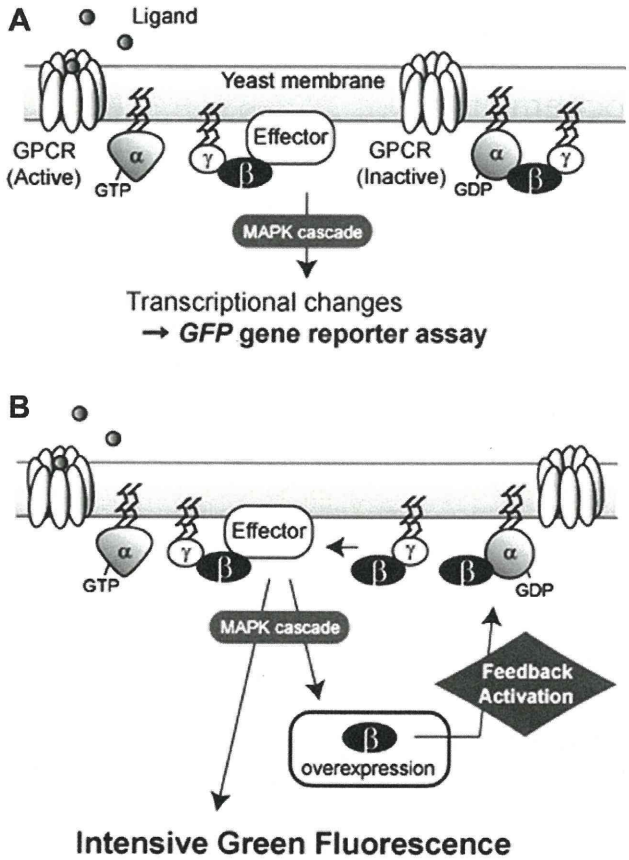

Fig.1. (A) Schematic outline of the strategy of *feedback signal activation* system commonly used to analyze agonist stimulation of GPCRs using the yeast pheromone signaling pathway. Agonistic ligand binding to the GPCR leads to activation of heterotrimeric G-proteins composed of Gpa1 (Gα), Ste4 (Gβ), and Ste18 (Gγ). The activated G-proteins subsequently dissociate into Gα and a Gβγ dimer. The Gβγ dimer induces activation of the MAPK cascade, resulting in expression of a *GFP* reporter gene. (B) Feedback signal activation approach for robust and highly sensitive detection of GPCR agonists. Ligand stimulation induces the expression of both *GFP* and *STE4* (Gβ) genes. This Gβ that is overexpressed in a signal-responsive manner competes with endogenous Gβ present in the Gαβγ heterotrimer for Gα binding. Such competition releases a free Gβγ complex that can amplify the weak signal caused by partial coupling between the heterologous GPCR and endogenous yeast G-protein. The resulting intense green fluorescence improves the sensitivity of heterologous GPCR signal detection.

yeast systems for analysis of human GPCR signaling is that the level of the signals transmitted from human GPCRs is commonly lower than that from the endogenous yeast GPCR due to inefficient coupling between the yeast G-protein and the human GPCR [10]. Thus, high signal-to-noise ratio in reporter gene assays is a critical factor in order to achieve powerful and reliable screening of human GPCR agonists. Therefore, a highly sensitive system that can detect reporter genes in yeast even in response to weak signals would be beneficial for screening of human GPCR agonists.

Here we describe a novel strategy to improve the sensitivity of detection of agonist-dependent signaling of a human GPCR that is expressed on a yeast cell surface. Because this strategy involves signal-induced expression of a gene encoding an activator (Gβ subunit) of the effector protein that is the output of yeast G-protein signaling, induction of this gene is expected to result in persistent activation of the MAPK cascade after signal initiation (Fig. 1B). Thus, agonist addition switches on "feedback signal activation" of yeast G-protein signaling. In the current study, we show the feasibility of this approach and its potency for the detection of human GPCR agonists.

Materials and methods

Strains, plasmids, and media

The genotypes of the *S. cerevisiae* strains and plasmids used in this study are outlined in Table 1. Yeast cells were grown in YPD medium containing 1% (w/v) yeast extract, 2% peptone, and 2% glucose, in SD medium containing 0.67% yeast nitrogen base without amino acids (Becton Dickinson, Franklin Lakes, NJ, USA) and 2% glucose, or in SDM71 medium (SD medium adjusted to pH 7.1 with 200 mM Mopso buffer) [11].

Construction of plasmids

To express the *STE4* gene (encoding Gβ) under the control of the pheromone-responsive *FIG1* promoter [11–15], the *STE4* gene was inserted into a plasmid that integrated into the yeast chromosome at a position upstream of the *HOP2* gene (P_{HOP2}:*HOP2* promoter region). Plasmid construction was as follows. The *STE4* gene was amplified from BY4741 [16] genomic DNA using the primers 5′-aaaaGTCGACatggactacaaggatgacgatgacaaggcagcacatcagatggactcgataacgt-3′ and 5′-aaaaGGATCCctattgataacctggagacc-3′ (restriction enzyme sites are in uppercase letters) and was inserted into the *SalI–BamHI* sites of pLMFIG-STE18-H [17], yielding the plasmid pLMFIG-STE4-H.

The plasmid used for expression of the human somatostatin receptor subtype 5 (hSSTR5) was constructed as follows. A DNA fragment encoding the *hSSTR5* gene was amplified from pGK-SSTR5-HA [11] using the primers 5′-ccccGTCGACatggagcccctgttcc cagc-3′ and 5′-ccccGAATTCtcacagcttgctggtctgca-3′ (restriction enzyme sites are in uppercase letters) and was inserted into the *SalI–EcoRI* sites between the *PGK1* promoter (P_{PGK1}) and the *PGK1* terminator (T_{PGK1}) on pGK423 [18], yielding the plasmid pHM-SSTR5 (Table 1).

Construction of yeast strains

Each DNA fragment was introduced into yeast cells using the lithium acetate method [19]. The DNA fragments containing *LEU2*-P_{FIG1}-*STE4*-T_{PGK1}-P_{HOP2} were amplified from pLMFIG-STE4-H using the primers 5′-atacaattaattgacatcagcagacagcaaatgcacttgatatacgcagctcgactacgtcgtaaggccg-3′ (corresponding to 50 nt of the region directly upstream of P_{HOP2}) and 5′-atctttcaaatagagcctgg-3′ and were used to transform MC-F1 [17]. The transformants were

Table 1
List of yeast strains and plasmids used in this study.

Strain or plasmid	Description	Reference source
Yeast strains		
BY4741	*MAT***a** *his3Δ1 ura3Δ0 leu2Δ0 met15Δ0*	[16]
MC-F1	BY4741 *fig1*::*FIG1-EGFP*	[17]
MC-F1B	MC-F1 P_{HOP2}::*LEU2*-P_{FIG1}-*STE4*	This study
IMFD-70	BY4741 *sst2Δ*::*AUR1-C ste2Δ*::*LEU2 fig1Δ*::*EGFP his3Δ*::P_{FIG1}-*EGFP far1Δ*	[11]
IMFD-70B	IMFD-70 P_{HOP2}::*URA3*-P_{FIG1}-*STE4*	This study
Plasmids		
pGK411	Yeast expression vector containing *PGK1* promoter, *CEN/ARS* origin, and *MET15* marker	[21]
pGK411-STE2	*STE2* in pGK411	[21]
pGK423	Yeast expression vector containing *PGK1* promoter, 2μ origin, and *HIS3* marker	[18]
pHM-SSTR5	*hSSTR5* in pGK423	This study

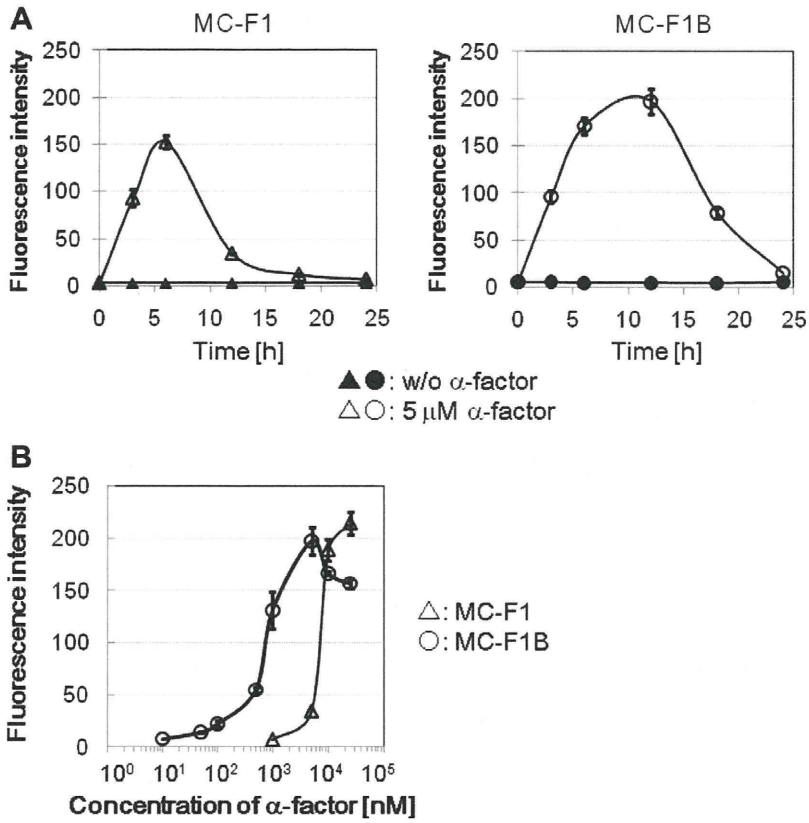

Fig.2. Fluorescence of a *GFP* reporter gene in response to agonist stimulation of the endogenous yeast Ste2 receptor in common and feedback activation strains. (A) Fluorescence of *GFP* reporter genes in the common activation yeast strain (MC-F1) and in the feedback signal activation strain (MC-F1B) with or without 5 μM α-factor stimulation. (B) Concentration–response curves of MC-F1 and MC-F1B to α-factor. The fluorescence intensities indicate the average values of 10,000 cells. The results are presented as means ± standard deviations of three independent experiments. w/o, without.

selected on SD solid medium without leucine but containing 20 mg/L uracil and histidine and 30 mg/L methionine (SD-Leu plate) to yield the MC-F1B strain (Table 1).

DNA fragments containing *URA3-*P_{FIG1}*-STE4-*T_{PGK1}*-*P_{HOP2} were constructed by overlap extension polymerase chain reaction (PCR) [20]. The *URA3*-containing fragment was amplified from pGK426 [18] using the primers 5′-cagacagcaaatgcac ttgatatacgcagcttcaatt-catcatttttttt-3′ (corresponding to 30 nt of the region directly upstream of P_{HOP2}) and 5′-gcgtttggttgatcattcaaggg taataactgatataa ttaaattgaagc-3′. The fragment containing P_{FIG1}*-STE4-*T_{PGK1}*-*P_{HOP2} was amplified from pLMFIG-STE4-H using the primers 5′-gcttcaatt-taattatatcagt tattaccttgaatgatcaaccaaacgccgatatagtc-3′ and 5′-atctttcaaatagagcctgg-3′. These two DNA fragments were ligated and used to transform IMFD-70 [11]. The transformants were selected on SD solid medium without uracil but containing 20 mg/L histidine and 30 mg/L leucine and methionine (SD-Ura plate) to yield the IMFD-70B strain (Table 1). The GPCR expression plasmids pGK411-Ste2 [21] and pHM-SSTR5 were used to transform both IMFD-70 and IMFD-70B strains.

Transcription assay using GFP fluorescent reporter gene

The Fig1p-EGFP (enhanced green fluorescent protein) fusion protein was used as a fluorescent reporter. The yeast cells were incubated at 30 °C, and their fluorescence intensities were then measured using a FACSCalibur equipped with a 488-nm air-cooled argon laser (Becton Dickinson). The data were analyzed using CELLQuest software (Becton Dickinson), and the average fluorescence intensity of 10,000 cells was defined as the geometric mean.

Fluorescence microscopic imaging

After incubation for 18 h at 30 °C, the yeast cells were washed and suspended in distilled water. The cell suspensions were observed using a BZ-9000 fluorescence microscope (Keyence, Osaka, Japan). Fluorescence images were acquired with a 510-nm band-pass filter for emission.

Results and discussion

General strategy

The aim of this study was to establish a sensitive and robust method for the detection of yeast G-protein signaling in order to enhance the usefulness of yeast-based systems for screening of agonistic ligands of human GPCRs. Our strategy was designed to trigger feedback activation of G-protein signaling through signal-induced expression of an artificial signal activator. The endogenous yeast Gβ subunit was selected as the signal activator because overexpression of Gβ constitutively activates the MAPK cascade through effector proteins even in the absence of agonists [22–24]. As shown in Fig. 1B, overexpression of a signal-responsive Gβ subunit is expected to result in the generation of free Gβγ complexes by competing with the endogenous γ-associated β subunit for binding to the α subunit. This competition would result in the release of free βγ dimers, which could then amplify the weak signal caused by partial coupling between the heterologous human GPCR and the endogenous yeast G-protein.

Based on the above theory, we constructed a recombinant yeast strain in which overexpression of the *STE4* gene that encodes the

yeast Gβ subunit can be induced by the signal-responsive *FIG1* promoter [11–15]. Initiation of G-protein signaling in this yeast by agonist stimulation was expected to lead to a feedback activation of G-protein signaling through this overexpressed Gβ subunit (Fig. 1B). We termed this strategy *feedback signal activation*. The endogenous yeast GPCR, the Ste2 receptor that interacts with endogenous yeast G-proteins, was first used to test our hypothesis that overexpression of a signal-responsive Gβ subunit would invoke feedback signal activation. Subsequently, the hSSTR5 was used to verify that such feedback signal activation allows highly sensitive and robust detection of agonists of human GPCRs on yeast cell surfaces.

Demonstration of feedback signal activation using the endogenous yeast GPCR

To validate our hypothesis, we constructed the yeast strain, MC-F1B, in which overexpression of the *STE4* gene is under the control of the signal-responsive *FIG1* promoter (Table 1). MC-F1B is derived from the MC-F1 yeast strain in which the chromosomal gene that encodes the endogenous yeast Ste2 receptor is intact and in which a *GFP* reporter gene is integrated at the *FIG1* locus to detect signaling in response to agonist stimulation (Table 1) [17].

The fluorescence of the *GFP* reporter gene in these two yeast strains was quantitatively evaluated during cultivation with 5 μM α-factor (an Ste2p agonist) in YPD medium. As shown in Fig. 2A, the modified strain (MC-F1B) displayed almost the same fluorescence intensity as the parental strain (MC-F1) over the first 6 h of cultivation. Subsequently, although the fluorescence of MC-F1 dramatically decreased due to inactivation of Ste2p signaling following receptor desensitization, the fluorescence of the MC-F1B strain was prolonged and GFP fluorescence was augmented for up to 12 h of cultivation. This result indicated that induction of the integrated *STE4* gene amplified signaling induced by Ste2p and that the overexpressed Gβ protein successfully invoked feedback activation of yeast G-protein signaling.

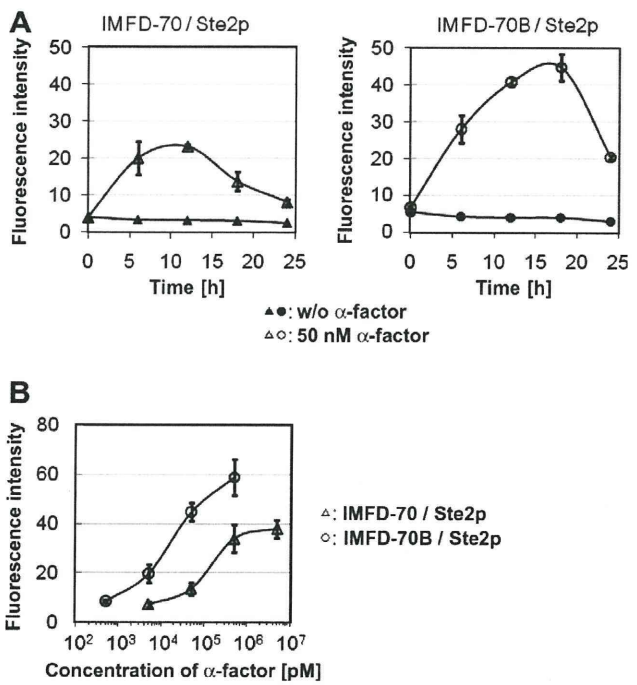

Fig.3. Fluorescence of a *GFP* reporter gene in response to agonist stimulation of common and feedback activation strains of yeast expressing the endogenous yeast Ste2 receptor gene from an episomal plasmid. (A) Fluorescence of the *GFP* reporter gene in the common activation strain (IMFD-70/Ste2p) and in the feedback signal activation strain (IMFD-70B/Ste2p) with or without 50 nM α-factor stimulation. (B) Concentration–response curves of IMFD-70/Ste2p and IMFD-70B/Ste2p to α-factor. The fluorescence intensities are the average values of 10,000 cells. The results are presented as means ± standard deviations of three independent experiments. w/o, without.

We further investigated the α-factor concentration dependency of this signaling to determine the ligand sensitivity of these strains. Data obtained after 12 h of cultivation were used to construct concentration–response curves (Fig. 2B). In the case of MC-F1, fluorescence intensity started to strongly increase at a concentration of approximately 5 μM α-factor and reached a maximum level at a concentration of 10–50 μM α-factor in a manner similar to that reported previously [25]. The half-maximal effective concentration (EC_{50}) value was 7 μM. In contrast, the fluorescence intensity of MC-F1B began to increase at a concentration of approximately 500 nM α-factor and reached its maximum at a concentration of 5 μM α-factor. The EC_{50} value was 800 nM. A similar difference in dose responses was also confirmed even when comparing the MC-F1 and MC-F1B at each optimal cultivation time (MC-F1 at 6 h and MC-F1B at 12 h) (see Supplementary Fig. S1 in supplementary material).

Although these results demonstrated that our feedback signal activation strategy is viable and can expand the detection limit of GPCR signaling to a lower concentration of agonistic ligand α-factor, the maximum intensity of GFP fluorescence at higher concentrations of α-factor did not increase (Fig. 2B). These data likely reflect the fact that the endogenous Ste2 receptor can couple efficiently with its intracellular cognate yeast G-protein in response to a native agonist, the α-factor.

Expression of the yeast Ste2 receptor using an episomal plasmid in a gene-deleted strain

Most heterologous GPCR assays in yeast systems are performed in several types of gene deletion mutants. Thus, the *SST2*-deleted strain confers hypersensitivity toward agonistic ligands, and the *FAR1*-deficient strain allows cell growth and plasmid recovery even in signal-activated states [21]. Moreover, the endogenous yeast *STE2* gene is often deleted to avoid competition of Ste2 receptor expression on the cell surface with that of human GPCRs [21]. Target GPCRs are commonly expressed from episomal plasmids in such yeast strains.

Unfortunately, however, signaling levels observed using episomal plasmid expression systems are frequently lower than those observed using chromosomal expression systems. One possible explanation of this difference might be due to the different cultivation conditions with YPD and SD media. To examine whether feedback signal activation can occur when using GPCRs expressed from episomal plasmids in strains with Ste2 and other deletions, we selected the IMFD-70 strain, which has triple deletion alleles (*sst2*Δ, *far1*Δ, and *ste2*Δ) and *GFP* reporter genes, as the parental yeast strain (Table 1) [11]. We then integrated the artificial signal activator *STE4* gene into the IMFD-70 chromosome, yielding the IMFD-70B strain (Table 1). To model episomal expression systems, the single-copy autonomous replicating plasmid for expression of the endogenous yeast Ste2 receptor (pGK411-STE2) [21] was introduced into both IMFD-70 and IMFD-70B strains.

The fluorescence of the *GFP* reporter gene of these two strains was then quantitatively evaluated during cultivation with 50 nM α-factor in SD selection medium. As shown in Fig. 3A, IMFD-70B/Ste2p (the feedback activation strain) maintained GFP fluorescence for a longer time (up to 18 h) than IMFD-70/Ste2p (the common activation strain, up to 12 h). This increased time of GFP fluorescence in the *STE4* gene-overexpressing strain is similar to the results of strains with chromosomal *STE2* genes. However, unlike strains that express chromosomal Ste2p, IMFD-70B/Ste2p dis-

played significantly higher fluorescence intensity than IMFD-70/Ste2p even before inactivation of signaling in IMFD-70/Ste2p (before 12 h). These results indicate that feedback signal activation was successfully invoked even when using an episomal plasmid expression system.

Concentration–response curves of these cells were constructed at 18 h of cultivation (Fig. 3B). Whereas the fluorescence intensity of IMFD-70/Ste2p started to increase from a concentration of approximately 50 nM α-factor and reached a maximum level at 500 nM α-factor, that of IMFD-70B/Ste2p gradually increased between concentrations of 500 pM and 500 nM α-factor. The EC_{50} values were 180 nM (IMFD-70/Ste2p) and 20 nM (IMFD-70B/Ste2p), respectively. A similar tendency in the difference of the dose responses was observed when comparing these strains at each optimal cultivation time (IMFD-70/Ste2p at 12 h and IMFD-70B/Ste2p at 18 h) (see Supplementary Fig. S2A). Increases in GFP fluorescence of the intensity observed in IMFD-70B/Ste2p have never been observed in non-feedback activation systems even at much higher concentrations of α-factor (data not shown). The concentration ranges of agonistic ligand required for signal activation in the episomal plasmid system were much lower than those required in the chromosomal system because of the hypersensitivity caused by the *SST2* deletion. In addition, both the detection limit and the maximum intensity of GFP fluorescence were apparently improved by feedback signal activation in the episomal system.

Feedback signal activation significantly improves the sensitivity of agonist detection, and the response to agonist stimulation, of the hSSTR5 receptor

Somatostatin (SST) is a cyclic neuropeptide known as a growth hormone release-inhibiting factor, and its receptors are therapeutic targets of acromegaly, Cushing's disease, and Alzheimer's disease [26–28]. To investigate whether feedback signal activation successfully rescues the partial activation of human GPCRs (which varies in strength depending on the coupling efficiency of the GPCR with yeast G-proteins) in yeast cells, we assayed SST stimulation of its GPCR, hSSTR5 [11].

An hSSTR5 expression plasmid (pHM-SSTR5) was introduced into IMFD-70 and IMFD-70B strains (Table 1). Each transformant was cultivated in SDM71 medium for signaling assay. Concentration–response curves of these cells were constructed by quantitative evaluation of the GFP fluorescence of both strains after 18 h of cultivation in the presence of several concentrations of SST (Fig. 4A). IMFD-70/hSSTR5 (the common activation strain) displayed a gradual increase in fluorescence intensity at concentrations of SST between 10 nM and 1 μM, and these responses were remarkably similar to those of a previous study [11]. However, the GFP fluorescence intensity of IMFD-70B/hSSTR5 (the feedback activation strain) was higher than that of the common activation strain at all SST concentrations tested. A similar result was obtained from the data at each optimal cultivation time (IMFD-70/hSSTR5 at 12 h and IMFD-70B/hSSTR5 at 18 h) (see Supplementary Fig. S2B). Moreover, compared with the GFP fluorescence induced by Ste2p in the IMFD-70 strain (the common activation strain), the level of hSSTR5 signaling was obviously lower, whereas the GFP fluorescence intensity of the Ste2p and hSSTR5 IMFD-70B strains (feedback activation strain) was equivalent (Fig. 4A). The EC_{50} value of the IMFD-70B/hSSTR5 strain was clearly improved as compared with that of the IMFD-70/hSSTR5 strain (from 55 to 8 nM). In addition, the advantage of IMFD-70B/hSSTR5 was supported by the fact that the EC_{50} value of the IMFD-70/hSSTR5 strain was almost similar to the value reported previously (109 nM) [11]. These results suggest that feedback signal activation compensates

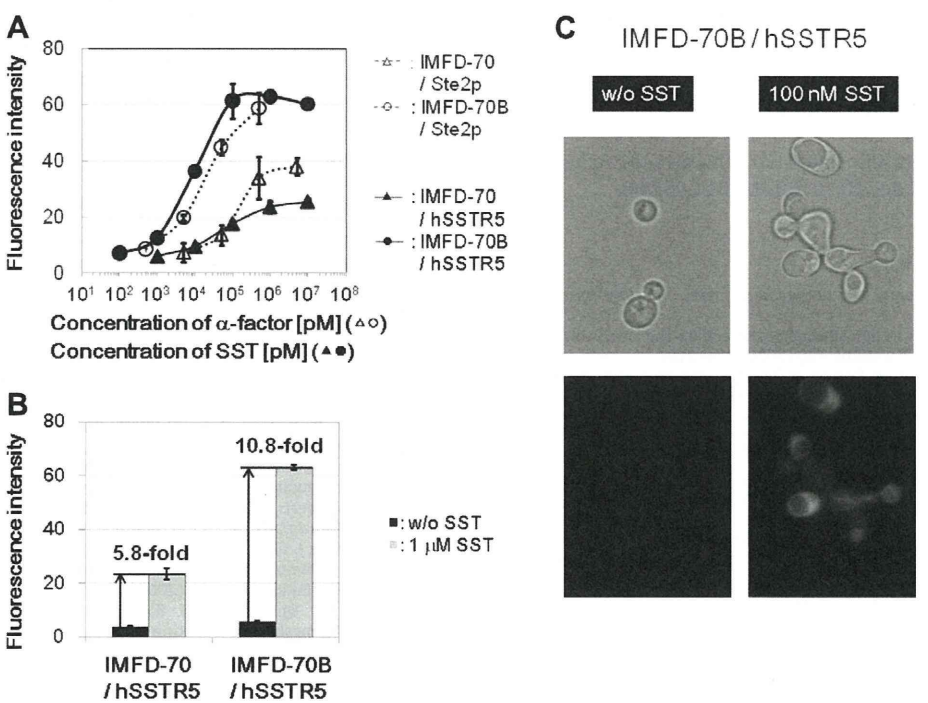

Fig.4. Fluorescence of a *GFP* reporter gene in response to agonist stimulation of common and feedback activation strains of yeast expressing hSSTR5. (A) Concentration–response curves of the common activation strain (IMFD-70/hSSTR5) and the feedback signal activation strain (IMFD-70B/hSSTR5) to the agonistic ligand SST. The dashed lines are overlays of the concentration–response curves of IMFD-70/Ste2p and IMFD-70B/Ste2p (data of Fig. 3B), which are included for comparative purposes. (B) Fluorescence of the *GFP* fluorescence reporter gene in IMFD-70/hSSTR5 and IMFD-70B/hSSTR5 with or without 1 μM SST stimulation. The fluorescence intensities are the average values of 10,000 cells. The results are presented as means ± standard deviations of three independent experiments. (C) Visualization of the green fluorescence of IMFD-70B/hSSTR5 with or without 100 nM SST. The upper photographs are differential interference contrast micrographs, and the lower photographs are fluorescence micrographs. w/o, without.

for inefficient receptor–G-protein coupling efficiency and significantly improves the sensitivity of agonist detection and the response to hSSTR5.

SST (1 μM) induced 5.8- and 10.8-fold increases over the signaling levels of unstimulated cells without agonistic ligands in the common and feedback activation strains, respectively (Fig. 4B). In addition, using a fluorescence microscope, we visually observed the changes in GFP fluorescence and morphology [29] in response to the SST-induced signal in the feedback activation strain (Fig. 4C). These results suggest that GFP fluorescence was specifically induced by agonists in the feedback activation strain and demonstrate the superiority and reliability of this approach for the detection of human GPCR agonists.

Conclusion

By expression of an artificial signal activator (Gβ) of the yeast G-protein signaling pathway, we have established a powerful approach for the detection of agonistic ligands of human GPCRs that are regarded as pharmaceutical and therapeutic targets. Using hSSTR5 as a model receptor, we demonstrated that feedback signal activation expands the detection limit for GPCR ligands and the maximum level of GPCR signaling in yeast. Our method is a reliable and versatile tool that could enhance the usefulness of yeast-based screening of agonistic ligands for a variety of human GPCRs.

Acknowledgments

This work was supported by a Research Fellowship for Young Scientists from the Japan Society for the Promotion of Science and, in part, by Special Coordination Funds for Promoting Science and Technology, Creation of Innovation Centers for Advanced Interdisciplinary Research Areas (Innovative Bioproduction Kobe), Ministry of Education, Culture, Sports, Science, and Technology (MEXT), Japan.

Appendix A. Supplementary data

Supplementary data associated with this article can be found, in the online version, at doi:10.1016/j.ab.2011.06.006.

References

[1] A.L. Hopkins, C.R. Groom, The druggable genome, Nat. Rev. Drug Discov. 1 (2002) 727–730.
[2] J. Giacomotto, L. Ségalat, High-throughput screening and small animal models: where are we?, Br J. Pharmacol. 160 (2006) 204–216.
[3] G.D. Stewart, C. Valant, S.J. Dowell, D. Mijaljica, R.J. Devenish, P.J. Scammells, P.M. Sexton, A. Christopoulos, Determination of adenosine A1 receptor agonist and antagonist pharmacology using *Saccharomyces cerevisiae*: implications for ligand screening and functional selectivity, J. Pharmacol. Exp. Ther. 331 (2009) 277–286.
[4] J. Minic, M. Sautel, R. Salesse, E. Pajot-Augy, Yeast system as a screening tool for pharmacological assessment of G-protein coupled receptors, Curr. Med. Chem. 12 (2005) 961–969.
[5] J.P. Manfredi, C. Klein, J.J. Herrero, D.R. Byrd, J. Trueheart, W.T. Wiesler, D.M. Fowlkes, J.R. Broach, Yeast α mating factor structure-activity relationship derived from genetically selected peptide agonists and antagonists of Ste2p, Mol. Cell. Biol. 16 (1996) 4700–4709.
[6] M.H. Pausch, M. Lai, E. Tseng, J. Paulsen, B. Bates, S. Kwak, Functional expression of human and mouse P2Y12 receptors in *Saccharomyces cerevisiae*, Biochem. Biophys. Res. Commun. 324 (2004) 171–177.
[7] E.V. Shusta, P.D. Holler, M.C. Kieke, D.M. Kranz, K.D. Wittrup, Directed evolution of a stable scaffold for T-cell receptor engineering, Nat. Biotechnol. 18 (2000) 754–759.
[8] M.J. Feldhaus, R.W. Siegel, L.K. Opresko, J.R. Coleman, J.M. Feldhaus, Y.A. Yeung, J.R. Cochran, P. Heinzelman, D. Colby, J. Swers, C. Graff, H.S. Wiley, K.D. Wittrup, Flow-cytometric isolation of human antibodies from a nonimmune *Saccharomyces cerevisiae* surface display library, Nat. Biotechnol. 21 (2003) 163–170.
[9] N. Fukuda, J. Ishii, S. Shibasaki, M. Ueda, H. Fukuda, A. Kondo, High-efficiency recovery of target cells using improved yeast display system for detection of protein–protein interactions, Appl. Microbiol. Biotechnol. 76 (2007) 151–158.
[10] G. Ladds, A. Goddard, J. Davey, Functional analysis of heterologous GPCR signalling pathways in yeast, Trends Biotechnol. 23 (2005) 367–373.
[11] S. Togawa, J. Ishii, A. Ishikura, T. Tanaka, C. Ogino, A. Kondo, Importance of asparagine residues at positions 13 and 26 on the amino-terminal domain of human somatostatin receptor subtype-5 in signalling, J. Biochem. 147 (2010) 867–873.
[12] N. Fukuda, J. Ishii, T. Tanaka, H. Fukuda, A. Kondo, Construction of a novel detection system for protein–protein interactions using yeast G-protein signaling, FEBS J. 276 (2009) 2636–2644.
[13] N. Fukuda, J. Ishii, T. Tanaka, A. Kondo, The competitor-introduced Gγ recruitment system, a new approach for screening affinity-enhanced proteins, FEBS J. 277 (2010) 1704–1712.
[14] J. Ishii, N. Fukuda, T. Tanaka, C. Ogino, A. Kondo, Protein–protein interactions and selection: yeast-based approaches that exploit guanine nucleotide-binding protein signaling, FEBS J. 277 (2010) 1982–1995.
[15] Y. Iguchi, J. Ishii, H. Nakayama, A. Ishikura, K. Izawa, T. Tanaka, C. Ogino, A. Kondo, Control of signalling properties of human somatostatin receptor subtype-5 by additional signal sequences on its amino-terminus in yeast, J. Biochem. 147 (2010) 875–884.
[16] C.B. Brachmann, A. Davies, G.J. Cost, E. Caputo, J. Li, P. Hieter, J.D. Boeke, Designer deletion strains derived from *Saccharomyces cerevisiae* S288C: A useful set of strains and plasmids for PCR-mediated gene disruption and other applications, Yeast 14 (1998) 115–132.
[17] N. Fukuda, J. Ishii, A. Kondo, Gγ recruitment system incorporating a novel signal amplification circuit to screen transient protein-protein interactions, FEBS J. (2011), doi:10.1111/j.1742-4658.2011.08232.x.
[18] J. Ishii, K. Izawa, S. Matsumura, K. Wakamura, T. Tanino, T. Tanaka, C. Ogino, H. Fukuda, A. Kondo, A simple and immediate method for simultaneously evaluating expression level and plasmid maintenance in yeast, J. Biochem. 145 (2009) 701–708.
[19] D. Gietz, A. St. Jean, R.A. Woods, R.H. Schiestl, Improved method for high efficiency transformation of intact yeast cells, Nucleic Acids Res. 20 (1992) 1425.
[20] S.N. Ho, H.D. Hunt, R.M. Horton, J.K. Pullen, L.R. Pease, Site-directed mutagenesis by overlap extension using the polymerase chain reaction, Gene 77 (1989) 51–59.
[21] J. Ishii, T. Tanaka, S. Matsumura, K. Tatematsu, S. Kuroda, C. Ogino, H. Fukuda, A. Kondo, Yeast-based fluorescence reporter assay of G-protein-coupled receptor signalling for flow cytometric screening: *FAR1* -disruption recovers loss of episomal plasmid caused by signalling in yeast, J. Biochem. 143 (2008) 667–674.
[22] S. Nomoto, N. Nakayama, K. Arai, K. Matsumoto, Regulation of the yeast pheromone response pathway by G protein subunits, EMBO J. 9 (1990) 691–696.
[23] M. Whiteway, L. Hougan, D.Y. Thomas, Overexpression of the STE4 gene leads to mating response in haploid *Saccharomyces cerevisiae*, Mol. Cell. Biol. 10 (1990) 217–222.
[24] K.L. Clark, D. Dignard, D.Y. Thomas, M. Whiteway, Interactions among the subunits of the G protein involved in *Saccharomyces cerevisiae* mating, Mol. Cell. Biol. 13 (1993) 1–8.
[25] J. Ishii, S. Matsumura, S. Kimura, K. Tatematsu, S. Kuroda, H. Fukuda, A. Kondo, Quantitative and dynamic analyses of G-protein-coupled receptor signaling in yeast using Fus1, enhanced green fluorescence protein (EGFP), and His3 fusion protein, Biotechnol. Prog. 22 (2006) 954–960.
[26] T. Saito, N. Iwata, S. Tsubuki, Y. Takaki, J. Takano, S.M. Huang, T. Suemoto, M. Higuchi, T.C. Saido, Somatostatin regulates brain amyloid β peptide Aβ42 through modulation of proteolytic degradation, Nat. Med. 11 (2005) 434–439.
[27] S.W. Lamberts, W.W. de Herder, E.P. Krenning, J.C. Reubi, A role of (labeled) somatostatin analogs in the differential diagnosis and treatment of Cushing's syndrome, J. Clin. Endocrinol. Metab. 78 (1994) 17–19.
[28] A. Ben-Shlomo, S. Melmed, Somatostatin agonists for treatment of acromegaly, Mol. Cell. Endocrinol. 286 (2008) 192–198.
[29] L. Yu, M. Qi, M.A. Sheff, E.A. Elion, Counteractive control of polarized morphogenesis during mating by mitogen-activated protein kinase Fus3 and G1 cyclin-dependent kinase, Mol. Biol. Cell 19 (2008) 1739–1752.

OPEN ACCESS Freely available online

PLoS one

Cell Wall Trapping of Autocrine Peptides for Human G-Protein-Coupled Receptors on the Yeast Cell Surface

Jun Ishii[1], Nobuo Yoshimoto[2,3], Kenji Tatematsu[2], Shun'ichi Kuroda[2,3], Chiaki Ogino[4], Hideki Fukuda[4], Akihiko Kondo[4]*

1 Organization of Advanced Science and Technology, Kobe University, 1-1 Rokkodai, Nada, Kobe, Japan, **2** Department of Structural Molecular Biology, Institute of Scientific and Industrial Research, Osaka University, 8-1 Mihogaoka, Ibaraki, Osaka, Japan, **3** Graduate School of Bioagricultural Sciences, Nagoya University, Furo, Chikusa, Nagoya, Japan, **4** Department of Chemical Science and Engineering, Graduate School of Engineering, Kobe University, 1-1 Rokkodai, Nada, Kobe, Japan

Abstract

G-protein-coupled receptors (GPCRs) regulate a wide variety of physiological processes and are important pharmaceutical targets for drug discovery. Here, we describe a unique concept based on yeast cell-surface display technology to selectively track eligible peptides with agonistic activity for human GPCRs (Cell Wall Trapping of Autocrine Peptides (CWTrAP) strategy). In our strategy, individual recombinant yeast cells are able to report autocrine-positive activity for human GPCRs by expressing a candidate peptide fused to an anchoring motif. Following expression and activation, yeast cells trap autocrine peptides onto their cell walls. Because captured peptides are incapable of diffusion, they have no impact on surrounding yeast cells that express the target human GPCR and non-signaling peptides. Therefore, individual yeast cells can assemble the autonomous signaling complex and allow single-cell screening of a yeast population. Our strategy may be applied to identify eligible peptides with agonistic activity for target human GPCRs.

Citation: Ishii J, Yoshimoto N, Tatematsu K, Kuroda S, Ogino C, et al. (2012) Cell Wall Trapping of Autocrine Peptides for Human G-Protein-Coupled Receptors on the Yeast Cell Surface. PLoS ONE 7(5): e37136. doi:10.1371/journal.pone.0037136

Editor: Debra Kendall, University of Connecticut, United States of America

Received December 16, 2011; **Accepted** April 13, 2012; **Published** May 18, 2012

Funding: This work was supported in part by a Grant-in-Aid for Scientific Research on Priority Areas (Life surveyor) from the Ministry of Education, Culture, Sports, Science and Technology (MEXT), the Regional Innovative Consortium Project of the Ministry of Economy, Trade and Industry (METI) and a Special Coordination Funds for Promoting Science and Technology, Creation of Innovation Centers for Advanced Interdisciplinary Research Areas (Innovative Bioproduction Kobe; iBioK) from the MEXT of Japan, and funded in part by AS ONE Corporation and the Naito Foundation. The funders had no role in study design, data collection and analysis, decision to publish, or preparation of the manuscript.

Competing Interests: This work was supported in part by AS ONE Corporation. This does not alter the authors' adherence to all the PLoS ONE policies on sharing data and materials.

* E-mail: akondo@kobe-u.ac.jp

Introduction

G-protein-coupled receptors (GPCRs) constitute a large superfamily of cell surface receptors [1]. In humans, these 7-transmembrane proteins respond to external stimuli to regulate various cellular processes including taste, smell, vision, heart rate, blood pressure, neurotransmission and cell growth [2]. All members of the guanine nucleotide binding protein family (G-proteins) share a common mechanism for signal transmission following GPCR-agonist binding [3]. This universal signaling mechanism has become a central tenet in G-protein research, and GPCRs have become major pharmaceutical targets for drug discovery [4].

The eukaryotic unicellular yeast, *Saccharomyces cerevisiae*, also shares the G-protein-mediated signal transmission mechanism with higher mammalian cells [3]. It is notable that *S. cerevisiae* offers a crucial advantage to simplify the study of GPCR signaling because it expresses only one kind of G-protein, which thereby avoids potential problems such as signaling cross-talk in mammalian cells [5–8]. Therefore, *S. cerevisiae* is a suitable host cell for the screening of functional residues in GPCRs [5,9,10].

Yeast cell-surface display technology is a powerful platform that enables proteins expressed in yeast to be tethered onto the cell surface [11–15]. This is accomplished by the use of "anchor" proteins that naturally localize on the cell surface in yeast cells. Typically, the gene encoding the target protein is fused to the anchor protein together with a secretion signal sequence at the N-terminus to both enable secretion of the fusion protein and to tether it firmly to the cell surface. As typical anchor proteins, the C-terminal domains of truncated α-agglutinin (Sag1p; a mannoprotein involved in sexual adhesion) and truncated Flo1p (a lectin-like cell-wall protein involved in flocculation) containing the glycosyl-phosphatidylinositol (GPI) anchor attachment signal sequence at the C-terminus are fused to the target protein at their N-termini [16,17]. Regarding other anchor proteins, the Flo1p flocculation functional domain without the GPI anchor attachment signal (FS anchor) permits the fusion of the target protein to both its N- and C-termini [18]. These anchor proteins are used to display the target proteins on the yeast cell wall. In contrast, periplasmic invertase (Suc2 anchor) can be fused to both the N- and C-termini of a target protein, enabling it to localize into the periplasmic space [19]. To date, yeast cell-surface display technology has been adopted for a broad range of applications including enzymatic catalysis, immune adsorption and protein engineering [16–18,20–23].

Here, we describe a unique concept using yeast cell-surface display technology to selectively track eligible peptides that present agonistic activity for human GPCRs. In our system, individual yeast cells expressing human GPCRs fulfill a series of roles from the manufacture of peptides to the sensing of agonistic activity. Briefly, yeast cells synthesize candidate peptides in fusion with

a secretion signal sequence and an anchoring motif. Agonistic peptides are capable of binding cell surface GPCRs that transduce the signal into the cell. Finally, the yeast traps the signaling peptide on its cell wall (Figure 1). Here, we use a yeast strain that is engineered to express a green fluorescent protein (*GFP*) reporter gene in response to GPCR activation. Therefore, stimulation by agonistic peptides can be recognized by the generation of a green fluorescence signal [3]. In principle, because signaling peptides are unable to diffuse to surrounding cells, our strategy has the potential to build autonomous signaling complexes on a cell-by-cell basis. Our peptide trapping method (cell wall trapping of autocrine peptides (CWTrAP) system) will allow the identification of lead peptides from combinatorial peptide libraries as starting points for drug screening.

Results and Discussion

To corroborate the viability of cell-surface display technology to track agonistic activity for GPCRs (CWTrAP system), we used α-factor pheromone, a natural ligand for the endogenous yeast 7-transmembrane GPCR, Ste2, which is specifically expressed in the **a**-type-strain [24]. In nature, α-type yeast strains secrete α-factor to induce mating signal transduction in the **a**-type strain by binding to the Ste2 receptor on its cell surface [25]. The ability of several types of protein motifs to anchor and transduce the autocrine α-factor were tested in the recombinant **a**-type yeast cells, which can express a *GFP* reporter gene in response to pheromone signaling (Figure 1). All constructs of fusion proteins that displayed α-factor peptides were designed to contain a Flag tag between the α-factor peptides and anchor proteins (Figure 2A and Table 1).

We used the IMG-4 yeast strain to display α-factor pheromone on its cell surface because this strain can monitor signaling levels through its endogenous Ste2 receptor via a *GFP* reporter gene (Table 1). To test our concept, we evaluated the C-terminal 320 aa of Sag1p (C-terminal half of α-agglutinin; AG) [16] and various lengths of truncated Flo1p derivatives (C-terminal 42, 102, 146 and 318 aa of Flo1p; Flo42, Flo102, Flo146 and Flo318) [17] as anchor proteins with GPI anchoring motifs (Figure 2A and Table 1). A recombinant yeast strain, engineered to express the α-factor autocrine peptide with a secretion signal sequence but lacking an anchor motif, robustly generated a higher green fluorescence signal than a strain harboring a mock plasmid (Figure 3A, Mock and Sec). Immunofluorescence staining of Flag-tagged α-factor peptide revealed no fluorescence on the surface of engineered yeast cells (Figure 3B, Sec). These results suggest that secreted α-factor could bind the endogenous Ste2 receptor and transduce the signal inside the yeast cells.

Next, we tested the cell wall trapping (CWTrAP) strategy for α-factor peptide with GPI anchoring motifs. All engineered yeast strains expressing α-factor peptides fused to the N-termini of the anchor proteins (AG and Flo42–318) with an inserted Flag tag (Figure 2A) successfully generated a green fluorescence signal (Figure 3A), confirming that the fusion peptide is able to activate signal transduction in yeast. Using GFP fluorescence intensity as an indicator of signaling strength, shorter anchor peptides appeared more capable of activating the GPCR (Figure 3A). The α-factor peptide fused to Flag and Flo42 exhibited higher responsiveness compared to α-factor lacking the anchor protein. This interesting result may arise from the transient enrichment of the GPI-anchored peptide on the yeast cell membrane, although the GPI-anchored peptide should be cleaved from the plasma membrane by phosphatidylinositol-specific phospholipase C (PI-PLC) and tethered on the cell wall [11–13].

Although shorter peptides tend to make detection of the Flag tag more difficult, due to the report that shorter peptides can bury the tag within the cell wall [17], we were able to confirm an anchor-dependent association with the yeast cell wall by immunofluores-

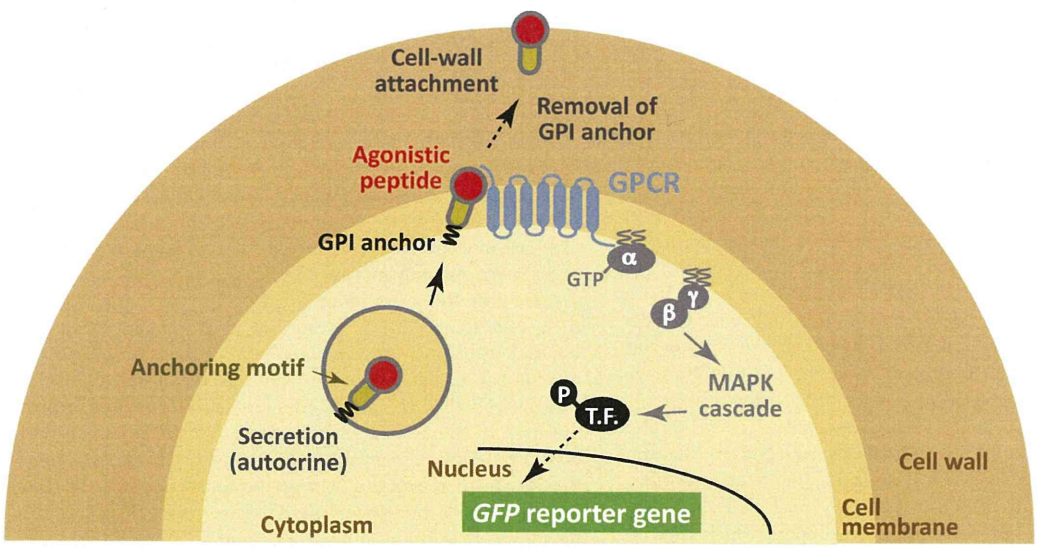

Figure 1. Schematic illustration of our concept using yeast cell-surface display technology to selectively track eligible agonistic peptides for human GPCRs by assembling the autonomous signaling complex within individual cells (cell wall trapping of autocrine peptides (CWTrAP) strategy). The candidate autocrine peptides fused with the anchoring proteins are processed via secretion pathways in engineered yeast cells. Their agonistic activities for heterologously-expressed human GPCRs are discerned on yeast cell membranes. Only when the peptide possesses objective agonistic activity, membrane-peripheral G-proteins promote intracellular signaling and induce transcription of the GFP reporter gene. Because the autocrine peptides are automatically trapped onto individual yeast cell walls, the captured peptides are unable to diffuse toward surrounding yeast cells that express the target human GPCR and any other peptides. T.F. indicates transcription factor.
doi:10.1371/journal.pone.0037136.g001

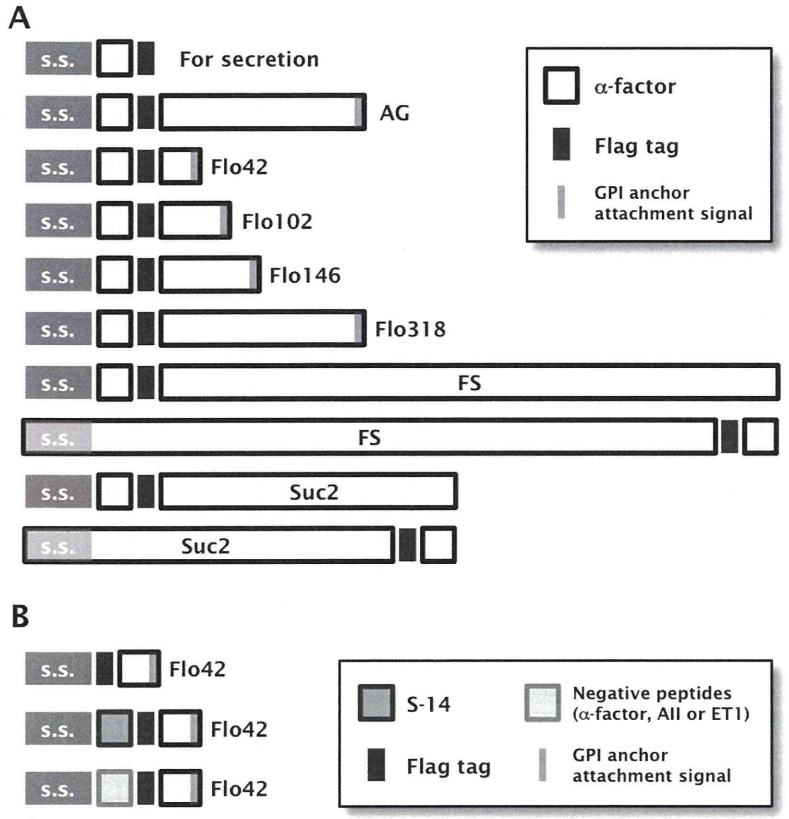

Figure 2. Schematic illustration of the fusion protein constructs used to display agonistic peptides on the yeast cell-surface. (A) Constructs for displaying α-factor peptides. AG: C-terminal half of α-agglutinin anchor. s.s.: secretion signal sequence. The pre-pro-region derived from α-factor was used as s.s. For the fusion of FS and Suc2 anchors to the α-factor peptides at their C-termini, the original s.s. encoded in the N-termini of Flo1p or Suc2p were used, respectively. The uppermost construct for secretion of α-factor peptide contains no anchoring motifs. All constructs contain the Flag tag. (B) Constructs for displaying S-14 by the Flo42 anchor. The upper construct displaying only Flag and Flo42 peptides was used as a negative control for the SSTR5 signaling assay. The middle and lower constructs displaying, respectively, eligible peptide (S-14) and negative control peptides (α-factor, All and ET1) by Flag–Flo42 fusion proteins were also used for the SSTR5 signaling assay.
doi:10.1371/journal.pone.0037136.g002

cence staining (Figure 3B). Because peptides anchored to the cell wall are unable to diffuse to surrounding cells, this result emphasizes the viability of our concept for the assembly of the autonomous signaling complex within individual yeast cells. Additionally, we verified that a subset of Flo42 was highly glycosylated (Figure S1); however, the agonistic activity of the α-factor peptide was unlikely to be affected by the posttranslational glycosylation of the anchor protein.

Next, we tested additional motifs that permit peptides to be fused to both the N- and C-termini of the anchor proteins. We replaced the GPI anchor proteins with the FS anchor [18] and the Suc2 anchor [19] (Figure 2A, Table S2 and Document S1). Signal transduction was more efficient when using the FS anchor, compared to the Suc2 anchor (Figure S2). These results show that agonistic peptides can be fused to both the N- and C-termini of anchor proteins. Even though the FS anchor (1099 aa) served as an efficient motif for transducing α-factor peptide signaling, we used the Flo42 anchor motif, whose molecular mass is much lower (Figure 2A), in all following experiments in order to minimize the possibility of steric hindrance.

To further demonstrate the viability of our concept, the IMFD-70 yeast strain, which can monitor signaling levels from recombinantly expressed heterologous GPCRs by a *GFP* reporter gene [5] (Table 1), was used to test if signal transmission from human GPCRs expressed on the yeast cell surface was possible. For these experiments, human somatostatin receptor subtype 5 (SSTR5), and the natural intramolecular-cross-linked cyclic peptide ligand, somatostatin 14 (S-14), were used [26,27].

To express the autocrine somatostatin and trap it on the yeast cell wall, we designed the S-14 peptide with an N-terminal secretion signal sequence and a C-terminal Flo42 anchor protein with a Flag tag (Figure 2B and Table 1). We constructed several negative controls by eliminating the S-14 peptide or by replacing it with agonistic peptides for other GPCRs (Figure 2B and Table 1). We expressed hemagglutinin (HA)-tagged human SSTR5 on the yeast cell surface using previously reported plasmids [5,6] (Table 1). We used these expression and mock plasmids to investigate the ability of the S-14 Flag Flo42 autocrine peptide to activate GPCR signaling (Figure 4).

As shown in Figure 4A, the engineered yeast strain concomitantly expressing SSTR5 HA and S-14 Flag Flo42 successfully induced *GFP* reporter gene expression, whereas the other control strains possessing either SSTR5 HA or S-14 Flag Flo42 did not. Similarly, a control strain expressing SSTR5 HA and the autocrine Flag Flo42 fusion protein lacking the S-14 peptide was unable to express a green fluorescence signal (Figure 4A).

Table 1. Yeast strains and plasmids used in this study.

Strain or plasmid	Relative feature	Source
Yeast strain		
BY4741	*MAT***a** *his3Δ1 leu2Δ0 met15Δ0 ura3Δ0*	[31]
IMG-4	BY4741 *fus1::FUS1-EGFP-*T_{GAPDH}*-HIS3 bar1Δ::LEU2 far1Δ::kanMX4*	This study
IMG-50	BY4741 *fus1::FUS1-EGFP-*T_{GAPDH}*-HIS3 sst2Δ::AUR1-C ste2Δ::LEU2*	[28]
IMFD-70	BY4741 *fig1Δ::EGFP his3Δ::*P_{FIG1}*-EGFP far1Δ sst2Δ::AUR1-C ste2Δ::LEU2*	[5]
Plasmid		
pESC-URA[a]	Expression vector containing *GAL1-GAL10* divergent promoter, 2μ origin and *URA3* marker	Agilent Technologies
pUESCαsf	pESC-URA, α-factor–Flag peptide expression (for secretion)	This study
pUESCαf-AG	pESC-URA, α-factor–Flag–AG[b] fusion protein expression (for display)	This study
pUESCαf-FLO42	pESC-URA, α-factor–Flag–Flo42 fusion protein expression (for display)	This study
pUESCαf-FLO102	pESC-URA, α-factor–Flag–Flo102 fusion protein expression (for display)	This study
pUESCαf-FLO146	pESC-URA, α-factor–Flag–Flo146 fusion protein expression (for display)	This study
pUESCαf-FLO318	pESC-URA, α-factor–Flag–Flo318 fusion protein expression (for display)	This study
pGK421[a]	Expression vector containing *PGK1* promoter, 2μ origin and *MET15* marker	[5,6]
pGK-SSTR5-HA	pGK421, SSTR5-HA human receptor expression	[5,6]
pGK426[a]	Expression vector containing *PGK1* promoter, 2μ origin and *URA3* marker	[36]
pGK42	pGK426, Flag–Flo42 anchor protein expression (for display)	This study
pGK-S1442	pGK426, S-14–Flag–Flo42[c] fusion protein expression (for display)	This study
pGK-alpha42	pGK426, α-factor–Flag–Flo42 fusion protein expression (for display)	This study
pGK-AII42	pGK426, AII–Flag–Flo42[d] fusion protein expression (for display)	This study
pGK-ET142	pGK426, ET1–Flag–Flo42[e] fusion protein expression (for display)	This study
pMHG-FIG1	Multi-copy reporter plasmid containing *FIG1* promoter, *GFP* reporter gene, 2μ origin and *HIS3* marker	[6]

All transcription products for display or secretion contain the secretion signal sequence of α-factor.
[a]The indicated vectors were used as mock controls.
[b]AG indicates C-terminal half of α-agglutinin anchor protein.
[c]S-14 encodes somatostatin 14 mature peptide.
[d]AII encodes angiotensin II mature peptide.
[e]ET1 encodes endothelin-1 mature peptide.
doi:10.1371/journal.pone.0037136.t001

These results demonstrate that autocrine activation of recombinant SSTR5 by binding of the S-14 peptide fused to the Flo42 anchor mediates pheromone signaling via endogenous peripheral G-proteins in yeast [5]. Furthermore, we were able to confirm the specificity of the S-14 peptide because three control peptides in which the S-14 peptide was replaced with the yeast Ste2 receptor agonist, α-factor, the human angiotensin receptor agonist, angiotensin II (AII), or the human endothelin receptor agonist, endothelin-1 (ET1), did not generate a green fluorescence signal (Figure 4B).

We confirmed the expression of SSTR5-HA receptor and S-14-Flag-Flo42 fusion protein by western blot analysis (Figure 5). Equal loading of the sodium lauryl sulfate (SDS)-extracted cell lysate fraction from each pellet was confirmed using anti-β-actin. SSTR5-HA receptor (anti-HA; lanes 2–4) and Flag-Flo42 anchor or S-14-Flag-Flo42 fusion proteins (anti-Flag; lanes 3–5) were successfully detected in the extracts of each appropriate transformant. The two unequal bands detected by the anti-Flag antibody in the Flag-Flo42 and S-14-Flag-Flo42 transformants likely represent the signal-cleaved and -uncleaved proteins, because the pre-pro-region derived from α-factor was used as the secretion signal sequence. We therefore tested the ability of the other active somatostatin isoform S-28 [26] and other secretion signal sequences (pre-region of α-factor and signal sequences derived from *S. cerevisiae* Suc2p and *Rhizopus oryzae* glucoamylase) to mediate signal transduction in the IMG-50 yeast strain. This strain has a slightly different genetic background to IMFD-70 (*FAR1*-intact strain [28], the description of the *far1Δ* allele can be found in Materials and Methods; Table 1), but the expression profiles of the *GFP* reporter genes remained essentially unchanged (Figure S3). Also, the insertion of GS linkers (GGGGS and GGGSGGGGS) between the S-14 peptide and Flag-Flo42 did not improve *GFP* expression (Figure S4). Because GPCR signaling has been reported to decrease plasmid retention even in the *far1Δ* yeast strain [28], false-negative signals (non-signaling cell cluster; Figure 4A, SSTR5-HA/S-14-Flag-Flo42) may be caused by plasmid loss. Because other secretion signal sequences and the insertion of GS linkers had no effect on expression of the *GFP* reporter gene, it is unlikely that a false-negative signal would be caused by steric hindrance of the S-14 peptide (Figure S3 and S4). Nevertheless, the presence of false-negative cells within an identical cell cluster implies that peptides captured on the cell wall have little influence on the surrounding cells (Figure 4, S3 and S4). Therefore, we demonstrated that peptides captured on the cell wall did not induce false-positive signals in surrounding non-target cells, even when two types of cells, one expressing the S-14-Flag-Flo42 (target cells) and the other expressing the Flag-Flo42 anchor lacking S-14 (non-target cells or surrounding cells), were mixed (Figure S5). Additionally, we successfully enhanced the weaker green fluorescence signal of the IMFD-70 strain expressing SSTR5-HA and S-14-Flag-Flo42 (Figure 4A) by concurrently introducing a multi-copy plasmid harboring the *GFP* reporter gene